



## Review

# A review of nanocarbons in energy electrocatalysis: Multifunctional substrates and highly active sites

Cheng Tang<sup>a</sup>, Maria-Magdalena Titirici<sup>b</sup>, Qiang Zhang<sup>a,\*</sup>

<sup>a</sup>Beijing Key Laboratory of Green Chemical Reaction Engineering and Technology, Department of Chemical Engineering, Tsinghua University, Beijing 100084, China

<sup>b</sup>Queen Mary University of London, School of Engineering and Materials Science, Mile End Road, E1 4NS London, UK

## ARTICLE INFO

## Article history:

Received 24 July 2017

Revised 9 August 2017

Accepted 15 August 2017

Available online 24 August 2017

## Keywords:

Nanocarbon  
Energy electrocatalysis  
Oxygen reduction  
Oxygen evolution  
Hydrogen evolution  
CO<sub>2</sub> reduction  
Electron structure  
Strong coupling effect  
Hierarchical structure  
Doping  
Defect  
Metal–air battery  
Fuel cell  
Water splitting

## ABSTRACT

Nanocarbons are of progressively increasing importance in energy electrocatalysis, including oxygen reduction, oxygen evolution, hydrogen evolution, CO<sub>2</sub> reduction, etc. Precious-metal-free or metal-free nanocarbon-based electrocatalysts have been revealed to potentially have effective activity and remarkable durability, which is promising to replace precious metals in some important energy technologies, such as fuel cells, metal–air batteries, and water splitting. In this review, rather than over-viewing recent progress completely, we aim to give an in-depth digestion of present achievements, focusing on the different roles of nanocarbons and material design principles. The multifunctionalities of nanocarbon substrates (accelerating the electron and mass transport, regulating the incorporation of active components, manipulating electron structures, generating confinement effects, assembly into 3D free-standing electrodes) and the intrinsic activity of nanocarbon catalysts (multi-heteroatom doping, hierarchical structure, topological defects) are discussed systematically, with perspectives on the further research in this rising research field. This review is inspiring for more insights and methodical research in mechanism understanding, material design, and device optimization, leading to a targeted and high-efficiency development of energy electrocatalysis.

© 2017 Science Press and Dalian Institute of Chemical Physics, Chinese Academy of Sciences. Published by Elsevier B.V. and Science Press. All rights reserved.



**Cheng Tang** received his B.S. degree in 2013 in the Department of Chemical Engineering, Tsinghua University, and is currently pursuing his Ph.D. there. His research interests focus on nanomaterials and energy electrocatalysis, including 3D graphene, hierarchical hybrids, oxygen reduction/evolution, and hydrogen evolution reactions.



**Magdalena Titirici** obtained her Ph.D. at the University of Dortmund, Germany. Between 2006 and 2012 she led the group “Sustainable Carbon Materials” at the Max Planck Institute of Colloids and Interfaces, Potsdam, Germany where she also did her “Habilitation”. In 2013 Dr. Titirici became an associate professor in Materials Science Queen Mary University of London. She was promoted to a full professorship in Sustainable Materials Chemistry in 2014. Dr. Titirici is the author of around 135 publications in the field of sustainable materials and green nanochemistry, several book chapters and one edited book. Her research interests include porous materials, hydrothermal carbonization, innovative utilization of biomass and

waste, biofuels, CO<sub>2</sub> sequestration, electrocatalysis in fuel cells as well as energy storage in secondary batteries and supercapacitors.

\* Corresponding author.

E-mail addresses: [zhang-qiang@mails.tsinghua.edu.cn](mailto:zhang-qiang@mails.tsinghua.edu.cn), [zhangqiangflotu@mail.tsinghua.edu.cn](mailto:zhangqiangflotu@mail.tsinghua.edu.cn) (Q. Zhang).



**Qiang Zhang** received his bachelor and Ph.D. degree from Tsinghua University, China in 2004 and 2009, respectively. After a stay in Case Western Reserve University, USA, and Fritz Haber Institute of the Max Planck Society, Germany, he joined in Tsinghua University, China at 2011. He held the Newton Advanced Fellowship from Royal Society, UK and the NSFC Young Scholar in China. His interests focus on energy materials, includes lithium–sulfur batteries, lithium metal anode, electrocatalysts, and 3D graphene based energy materials. Dr. Zhang is the author of around 200 publications in the field of advanced energy materials, 5 book chapters, and 1 edited book. His citation is over 11,000 times and his h-index is 56 now.

## 1. Introduction

The ultimate goal of the future energy scenario is to replace fossil fuels with sustainable and renewable energies, including solar, wind, hydro and geothermal heat [1,2]. To efficiently and reliably utilize these energies in transportation or stationary manners, advanced energy storage and conversion technologies are prerequisite, such as fuel cells [3,4], water splitting [5], solar cells [6], lithium ion batteries [2], lithium–sulfur batteries [7], metal–air batteries [8], supercapacitors [9]. Especially, photo-/electrocatalytic water splitting use solar or electric energies produced from renewable sources to generate clean  $H_2$ , and then fuel cells directly convert the chemical energy stored in hydrogen into electricity on demand for next-generation sustainable energy system [10–12]. Metal–air batteries (e.g., lithium–air battery [13], and zinc–air battery [14]) can utilize the inexhaustible oxygen from air as the reactant in breathing cathodes like that in fuel cells, and therefore leading to much higher theoretical energy densities than current commercialized batteries. Tremendous efforts have been made to improve the performances of these energy storage and conversion technologies [15,16], in which electrochemistry plays the critical role with a series of electrocatalysis, including the oxygen reduction reaction (ORR) [17–19] at the cathode of metal–air batteries or fuel cells (Fig. 1), oxygen evolution reaction (OER) [20,21] and hydrogen evolution reaction (HER) [22] at the anode and cathode of water electrolyzers (Fig. 1), as well as emerging  $CO_2$  reduction [23–25] in solid oxide electrolysis cells, liquid fuel conversion devices, and other energy catalysis devices.

However, these heterogeneous electrocatalytic reactions involve multi-step proton-coupled electron transfer and only occur at triple-phase boundary regions, leading to sluggish kinetics and urgent requirement of effective electrocatalysts. After decades of research, it has been well demonstrated nanocarbon materials are

of progressively increasing importance in energy electrocatalysis [26]. Various nanocarbons have been developed and revealed to bring about exciting possibilities, including the low-dimensional basic members (carbon nanotubes (CNTs), graphene, fullerene, and their derivatives), doped or functionalized nanocarbons, and hybrid or nano-architected materials [27]. For the commercial and state-of-the-art precious metal-based catalysts (Pt/C, Ir/C,  $IrO_2$ ,  $RuO_2$ , etc.), the employment of nanocarbons instead of routine carbon black (CB) can enhance the metal utilization, reduce the metal loading, enhance the stability and fuel-selectivity [27]. When strongly coupled with certain inorganic or organic nanomaterials, the nanocarbons can serve as multifunctional substrates to accelerate the 3D electron and mass transfer, modify the composite growth, endow inter-component charge transfer, bring about confinement effects, or assembly into self-supported electrodes, resulting in significantly enhanced performances [28,29]. More directly, the functionalized nanocarbons with specific heteroatom doping, hierarchical structure, edge sites, intrinsic topological defects, or metal–nitrogen–carbon moieties are demonstrated to be outstanding electrocatalysts and even comparable to precious metals. Nanocarbon materials have witnessed and promoted the development of energy materials and electrocatalysis far more than classical carbon and other materials. This is contributed from the unique size/surface-dependent and facily tunable properties which are critical for the electrocatalytic performances, such as the regulation of electronic structures through heteroatom doping, the adaption of hierarchical porosity by engineering integration of building blocks, and the modulation of surface chemistry through functional groups [27].

Up to date, numerous nanocarbon-based materials with distinct properties and structures have been proposed to replace the precious metal catalysts aiming at high-efficient and cost-effective energy electrocatalysis, including ORR, OER and HER [30,31]. Whereas, the research is dominantly based on trial-and-error approaches and the dazzling achievements confuse the further targeted improvement with respect to active origin [32], material design [33–35], electrolyte optimization [36], and device integration [37,38]. The resultant electrocatalytic performance of nanocarbon-based materials is strongly related to the intrinsic properties, active sites, hierarchical porosities, and hybrid structures. Many excellent reviews on related topics have been already published, including carbon-supported precious metal catalysts [39], carbon-based metal-free catalysts [31,40,41], strongly coupled carbon/inorganic hybrids [28,42], catalytic activity origins and engineering principles [40,43–45].

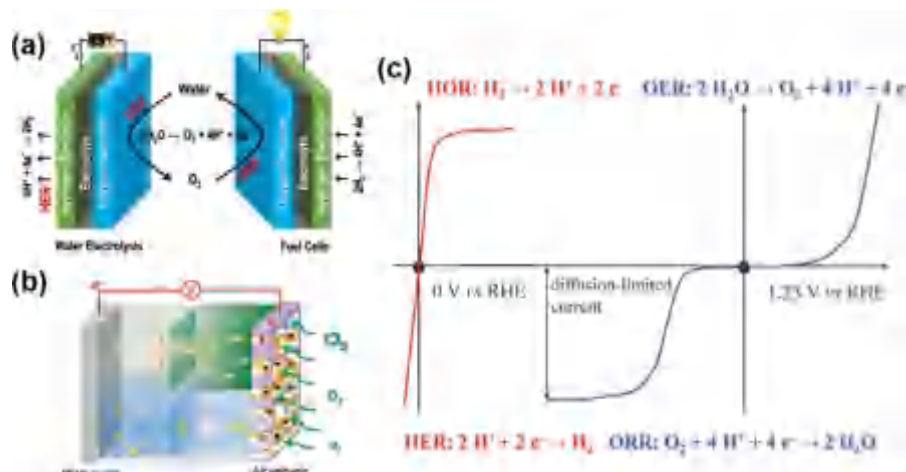


**Fig. 1.** (a) Schematic illustration of water splitting, fuel cells [43], and (b) metal–air batteries [46] with specific electrocatalysis. (c) Typical polarization curves of hydrogen-involving and oxygen-involving reactions [47].

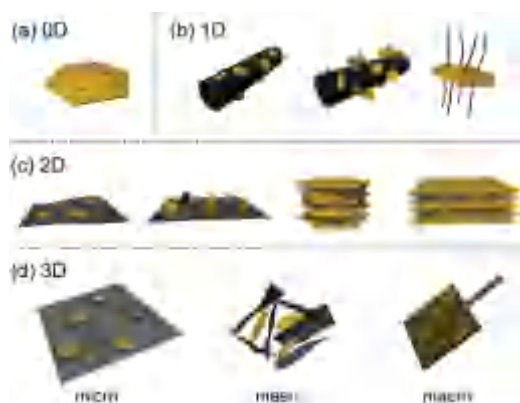


**Fig. 2.** Scheme of strongly coupled nanocarbon/inorganic nanomaterial hybrids with different nanostructures, including (a) 0D carbon quantum dots, (b) 1D CNTs, (c) 2D graphene, and (d) 3D graphene framework, which can be further classified into micro-, meso-, and macro-scale hybrids according to the structure of graphene substrates [29].

In this review, rather than giving a complete overview over all recent progress, we will focus on the different roles of nanocarbons and material design strategies to utilize nanocarbons in the field of energy electrocatalysis. The multifunctionalities of nanocarbon substrates and the activity origins of nanocarbon catalysts are discussed systematically in order to provide an in-depth digestion of previous achievements and afford bases for a more rational and effective utilization of nanocarbon materials. More attention will be paid to the efficient methods for material synthesis, the relationship between structure and activity, and the optimization principles for nanocarbon-based electrocatalysts. We hope this review is able to inspire more insights for mechanism understanding, material design, and device optimization, leading to a targeted and high-efficiency development of sustainable energy electrocatalysis.

## 2. Nanocarbons as multifunctional substrates

Compared with traditional carbon materials, nanocarbons always exhibit higher electrical conductivity, larger surface area, tunable structural hierarchy, ultra-thin graphitic layer, and low-dimensional properties [48,49]. These unique features render nanocarbons with multifunctionalities to strongly couple with other catalytically active components, and result in significantly enhanced performances. Several typical structures of the nanocarbon/active component hybrids are shown in Fig. 2 according to the type of nanocarbon materials [29].

In many cases, the highly active components (such as metal oxide/hydroxide/sulfide) are poorly conductive and in the powdery form, resulting in high charge transfer resistance, low utilization efficiency, inevitable particle aggregation and limited stability of catalysts. The use of nanocarbon materials can reduce these drawbacks. Dai's group firstly reported the  $\text{Co}_3\text{O}_4/\text{graphene}$  hybrid as bifunctional ORR/OER catalysts [50] and NiFe layered double hydroxide (LDH)/CNT hybrid for OER [51]. The introduction of nanocarbon components substantially increased the catalytic activity of pristine active components and led to superior stability to precious metals, attributed to the enhanced electron/mass transport and synergetic chemical coupling effects. Additionally, the functional groups on nanocarbon surface together with the micro/mesoporous morphology can modify the incorporation of active components, benefit the stable dispersion of catalytic active nanoparticles and improve the utilization efficiency. The strongly coupled interface or confinement effect can effectively manipulate the electron structures and adsorption energy. Such strongly

coupled interface is also confirmed in other multi-electron reactions in rechargeable batteries [52,53].

Furthermore, the low-dimensional nanocarbon materials provide feasibility to construct advanced 3D interconnected and free-standing scaffolds with smooth pathways for full penetration of electrolyte and rapid gas emission. In this section, we will summarize the recent progress according to these functionalities and roles, aiming at a clear description of how to utilize nanocarbons in high-efficiency hybrid electrocatalysts.

### 2.1. Accelerate the electron and mass transport

CNTs, graphene, and carbon quantum dots have been widely employed to strongly couple with active components via direct growth or post-treatment, aiming at accelerating the electron and mass transport and improving the catalytic performances [51,54–59].

Graphene, especially the reduced graphene oxides, is the most favorable substrate due to the high surface area, 2D lamellar structure, abundant functional groups on surface, and facility to be assembled into 3D porous frameworks. As shown in Fig. 3(a and b), a hydrogel-based OER electrocatalyst was fabricated via the incorporation of NiCo hydroxides into N-doped graphene hydrogels [60]. The graphene was assembled into a well-developed 3D interconnected porous network after hydrothermal treatment and then sheet-like hydroxide species were heterogeneously deposited onto graphene sheets. The dual active sites from N-doping and NiCo species, and high wettability of hydrogels contributed to excellent catalytic efficiency and great durability, much better than that of the state-of-the-art  $\text{IrO}_2$  catalysts (Fig. 3(c)). Moreover, the graphene provided 3D highly conductive network and well-defined macro/mesoporosity, leading to effective charge and mass transport. The catalytic current was less affected by scan rates (Fig. 3(d)), suggesting the importance of 3D architecture for efficient transport and improved performance [60].

Conductive and porous carbon materials have been selected to serve as the support for Pt-based nanoparticles for a long time. Carbon black (Vulcan XC 72) is still the main support presently used in commercial fuel cells [27,39]. On one hand, the uniform pore structure can limit the nanoparticle size, protect them against detachment, aggregation, and dissolution, and also facilitate mass diffusion. On the other hand, the conductive network connects electrochemically isolated Pt nanoparticles, reduces the resistance, and improves the Pt utilization efficiency. However, for those nanostructured carbon substrates, the porosity and conductivity are always interrelated and mutually influenced. Alternatively, single-walled carbon nanotubes (SWCNTs) [61] and graphene [62] are revealed to be more favorable substrates. Compared with commercial Pt/CB catalysts, the Pt/SWCNT exhibited much higher utilization efficiency (93% versus 34%), 3 times higher electrochemically active surface area (ECSA), more positive potential, and greatly enhanced electrocatalytic activity [61]. Besides, a 3-fold higher diffusion rate of reactants was observed, which was contributed to the ballistic diffusion occurring inside SWCNTs [61]. A better balance between the conductivity and porosity can be achieved using the graphene-based mesoporous carbon (G-mC) as substrate [62]. The mesoporous carbon layer was fabricated via carbonization of sucrose with mesoporous silica as template on both sides of graphene (Fig. 3(e)). The presence of graphene remarkably increased the electrical conductivity, and the mesoporous surface protected Pt nanoparticles against aggregation, encapsulation, and detachment (Fig. 3(f)), and reduced the diffusion path of electrolytes as well. As a result, the electrocatalytic activity, durability and utilization of Pt/carbon catalysts was highly improved [62].

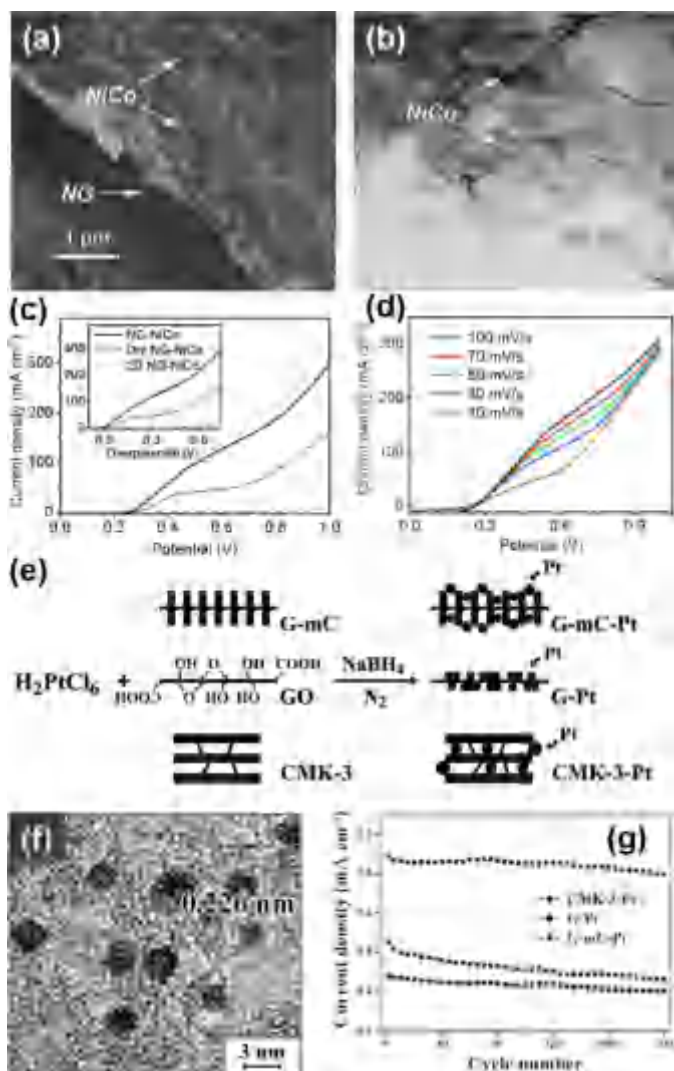


**Fig. 3.** Nanocarbons accelerate the electron and mass transport. (a) SEM and (b) TEM images of NG-NiCo. (c) Linear sweep voltammetry (LSV) plots obtained at  $50 \text{ mV s}^{-1}$  in  $0.10 \text{ M KOH}$ . (d) LSV plots obtained at different scan rates [60]. (e) Schematic illustration of the synthesis of different Pt/carbon catalysts. (f) TEM image of G-mC-Pt. (g) Methanol oxidation peak current as a function of the cycle number [62].

## 2.2. Modify the incorporation of active components

In regards to the strongly coupled hybrids of nanocarbons and active components, the enhanced catalytic performance is always achieved due to the active sites from active components and/or nanocarbons [63,64], and the improved electrical conductivity and mass transport from nanocarbons [65–67]. Such concept is widely accepted when carbon materials serve as hosts to accommodate active materials in various batteries [68–73] and supercapacitors [74–77]. Additionally, the nanocarbons can also play important roles to directly and significantly modify the obtained morphologies and properties of active components during the composite/hybrid fabrication, leading to optimal structure and performances [78–84].

Zhang's group proposed the spatial confine strategy to facilitate manipulate the hybridization and improve the catalytic performance of nanocarbon/inorganic systems [57,85–87]. A nitrogen-doped mesoporous graphene framework was fabricated by templated growth and employed as the substrate (Fig. 4(a)) [57]. Both nitrogen dopants and topology-induced defects of graphene

contributed to the defect-anchored nucleation, and then the mesopores served as nanoreactors for spatially confined growth, resulting in strongly coupled and uniformly dispersed nano-sized NiFe LDHs (Fig. 4(b and c)). Consequently, the as-obtained NiFe LDH/graphene hybrid was demonstrated to outperform the commercial Ir/C catalysts for OER, with significantly higher activities (overpotential required for  $10 \text{ mA cm}^{-2}$ :  $\sim 337 \text{ mV}$ ), improved kinetics (Tafel slope:  $\sim 45 \text{ mV dec}^{-1}$ ), and enhanced durability for oxygen evolution in alkaline conditions. This unique structure provided a nice platform for the study of catalytic mechanism of the NiFe LDHs [85] and can be generalized to other nanocarbon materials or active components, such as graphene/CNT hybrids [86] and transition metal hydroxysulfides/oxy-sulfides [87].

In addition to the inorganic active components (e.g., metal [89], alloys [90,91], oxides [92,93], carbides [94], sulfides [95], hydroxides [96–98], hydrofluoride [99], hydroxysulfides [87], and oxysulfides [100], etc.), nanocarbon materials also afford favorable surfaces for the tunable deposition of organic active components, such as graphitic carbon nitrides (g-C<sub>3</sub>N<sub>4</sub>) [101–103], metal organic frameworks [104], covalent organic framework [105,106], metal porphyrins/phthalocyanines [107,108], etc. For instance, metal porphyrin clusters can be *in-situ* immobilized on partly reduced graphene oxide, leading to evenly distributed nanoparticles via  $\pi$ - $\pi$  stacking interactions, hydrogen bonding, and electrostatic interactions [107]. The strong  $\pi$ - $\pi$  interactions between cobalt phthalocyanine (CoPc) and CNTs endowed effective anchoring of CoPc molecules on CNT surface under sonication and magnetic stirring in *N,N*-dimethyl formamide [88]. The as-obtained CoPc/CNT hybrid resembled the morphology of original CNTs without any aggregated CoPc particle (Fig. 4(d)). This uniform coverage and strong anchoring of CoPc on CNTs enabled a high degree of catalytic site exposure and rapid electron transfer, and minimized the exposure of carbon surface and CoPc detachment from electrode. Therefore, the CoPc/CNT hybrid catalyst exhibited exceptional catalytic performance for CO<sub>2</sub> reduction to CO. A high current density over  $10 \text{ mA cm}^{-2}$  with a Faradaic efficiency over 90%, corresponding to a turnover frequency of  $2.7 \text{ s}^{-1}$  was obtained at an overpotential of  $0.52 \text{ V}$  in  $0.10 \text{ M KHCO}_3$ .

Single-atom electrocatalysts are attracting increasing attention recently, contributed to the high activity, stability, selectivity, and 100% atom utilization [109,110]. However, there is still a grand challenge to facilitate and controllably synthesize highly dispersed single atoms instead of nanoparticles due to the tendency of metal atom fusion/aggregation. Nanostructured carbon materials and surface engineering strategies bring out new vigor into materials science. g-C<sub>3</sub>N<sub>4</sub> was demonstrated as an excellent platform to coordinate a variety of metals for superior ORR/OER bifunctional catalysts [111]. After acid leaching, the metal was dominantly remained in the form of single atoms or clusters, with precise metal-N<sub>2</sub> coordination moieties [111]. Analogously, the intrinsic structural defects in graphene were also promising to be utilized for generating atomically dispersed Co-N<sub>x</sub>-C active sites via defect engineering [112]. Besides, atomically dispersed Fe-N<sub>x</sub> species can be achieved on N,S co-decorated carbon layers by coating CNTs with 2,2-bipyridine and Fe salts, followed by pyrolysis and acid leaching [113]. The addition of S salts (SCN<sup>-</sup>) was revealed to be critically beneficial for the synthesis of atomic active sites due to the improved etching efficiency [113]. Most recently, Li's group described a cage-encapsulated-precursor pyrolysis strategy to fabricate isolated single-atom Fe/N-doped porous carbon (Fe-ISAs/CN) with a high Fe loading up to 2.16 wt% [114]. Both metal organic framework [115–120] and covalent organic framework [105] are considered as promising precursor for rational dispersion of metal into carbon scaffolds. Zeolitic imidazolate frameworks (ZIF-8) with a cavity diameter of  $11.6 \text{ \AA}$  were employed as the molecular-scale cages to encapsulate and separate metal precursor Fe(acac)<sub>3</sub>

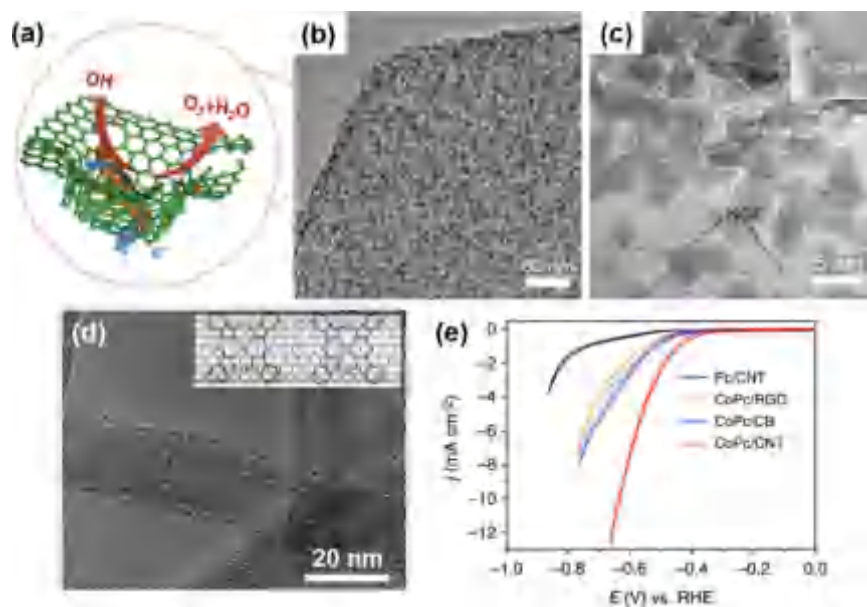


**Fig. 4.** Nanocarbons modify the incorporation of active components. (a) Scheme and (b, c) TEM images of the spatially confined growth of nano-sized NiFe LDHs in mesoporous graphene framework [57]. (d) TEM image of cobalt phthalocyanine/CNT hybrid, and (e) cyclic voltammograms obtained at  $5 \text{ mV s}^{-1}$  for  $\text{CO}_2$  reduction [88].

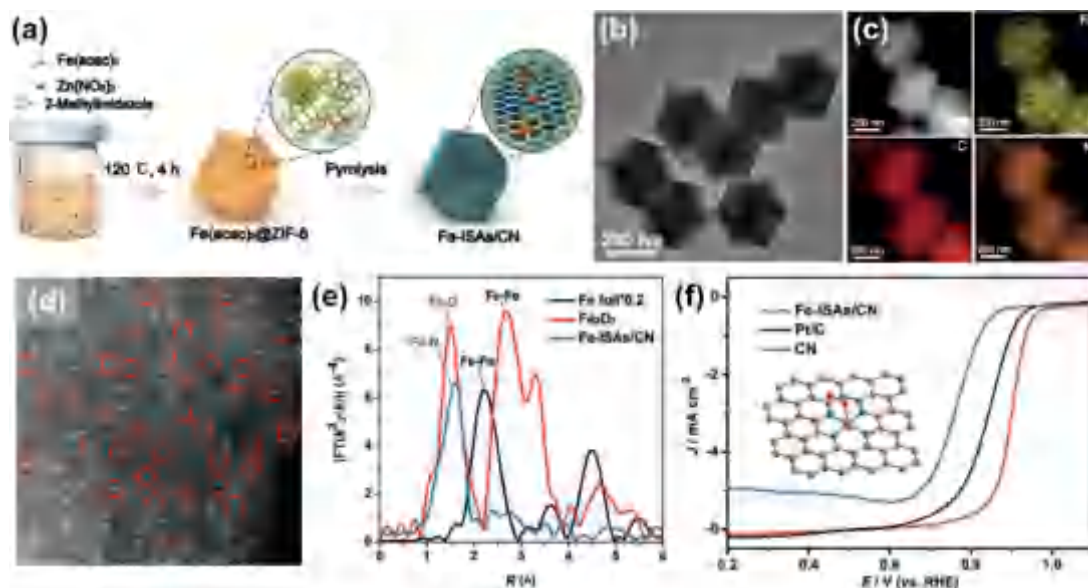


**Fig. 5.** Nanocarbons modify the incorporation of active components toward atomic active sites. (a) Scheme of the fabrication of Fe-ISAs/CN. (b) TEM image, (c) HAADF-STEM image and corresponding element maps of Fe-ISAs/CN. (d) HAADF-STEM image of Fe-ISAs/CN with single Fe atoms highlighted by red circle. The size of the TEM image is  $5.2 \text{ nm} \times 5.2 \text{ nm}$ . (e) Fourier transform of the Fe K-edge of Fe-ISAs/CN compared with Fe foil and  $\text{Fe}_2\text{O}_3$  [114].

(molecular diameter  $\sim 9.7 \text{ \AA}$ ) [114]. After high-temperature pyrolysis under Ar, the ZIF-8 transformed into nitrogen-doped porous carbon, and  $\text{Fe}(\text{acac})_3$  was reduced to isolated single iron atoms anchored on nitrogen species in each cage (Fig. 5(a)). Both scanning transmission electron microscope (STEM) and X-ray adsorption fine structure (XAFS) characterizations confirmed that the Fe atoms were atomically dispersed on nitrogen-doped carbon, and were four-fold coordinated by N atoms (Fig. 5(b–e)). Impressively, the as-obtained Fe-ISAs/CN was revealed to exhibit outstanding ORR activity with  $58 \text{ mV}$  more positive half-wave potential than Pt/C, and good methanol tolerance and stability (Fig. 5(f)).

### 2.3. Manipulate the electron structures

The Sabatier principle is always followed to elucidate the reaction mechanism and optimize the catalysts for heterogeneous

electrocatalysis involving oxygen and hydrogen [47]. This principle claims that the bonding of reaction intermediates (e.g.,  $\text{OOH}^*$ ,  $\text{H}^*$ , etc.) to the favorable electrocatalyst surface should not be too weak or too strong, leading to the optimal catalyst at the peak of activity volcano plots. Generally, the adsorption energies of intermediates are suggested to be determined by the electron structure of the catalyst surface, such as the  $d$ -orbital of the metal catalysts and valence orbital of the carbon catalysts [44].

To optimize the adsorption energies and climb to the volcano peak, various strategies have been developed, among which the electron structure manipulation of active components is found to be significantly attractive [100,121]. The interfacial charge transfer in alloy nanoparticles, between metal and capping ligand/carbon supports, and in heteroatom-doped carbon skeletons are exploited to effectively engineer the electronic energy structures, modify the adsorption properties, and promote apparent activities [45,122].

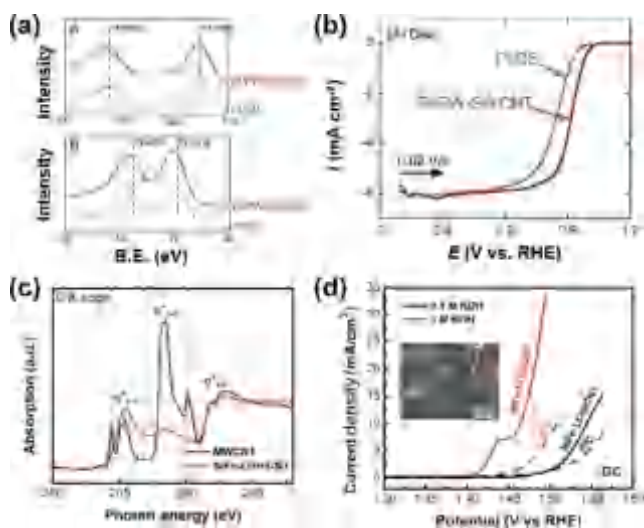


**Fig. 6.** Nanocarbons manipulate the electron structures of active components via interfacial charge transfer. (a) XPS of Pt of Pt/polymer-wrapped SWCNTs and Pt/CB, and (b) ORR current densities in  $O_2$ -saturated 0.10 M  $HClO_4$  [61]. (c) C K-edge XANES spectra of NiFe LDH/CNT and pure CNTs. (d) OER current densities of NiFe LDH/CNT measured on glass carbon electrode with a catalyst loading of  $0.20 \text{ mg cm}^{-2}$  [51].

For instance, the Pt in the SWCNTs supported catalyst exhibited a shift about 0.4 eV to the higher binding energy in both 4d and 4f electrons compared with the CB supported one, suggesting the more effective role of SWCNTs on modifying electronic properties and enhancing the ORR activity (Fig. 6(a and b)) [45]. The electron-deficiency of Pt could be finely tuned through synthesis methods and the different electron donation-acceptance behaviors between Pt and graphitic/pyridinic nitrogen [123]. In various NiFe LDH/nanocarbon hybrids, the strong interfacial interaction was clearly revealed by X-ray photoelectron spectroscopy (XPS) [57] and X-ray absorption near edge structure (XANES) [51], leading to the formation of metal–O/N–carbon bonding, modification of electron structures and thus enhancement of catalytic activities (Fig. 6(c and d)). Up to date, the synergetic chemical coupling effect and interfacial charge transfer have been widely reported in different hybrid systems, such as graphene/ $Co_3O_4$  [50],  $g-C_3N_4/Ti_3C_2$  [103], graphene quantum dots/graphene nanoribbons [124], polysulfides/doped carbon [125], and so on. The cooperative interface (e.g. “lithophilic” nitrogen-doped graphene frameworks and “sulfiphilic” NiFe LDH) is also proposed to synergistically afford bifunctional Li and S binding to regulate the intermediate distribution in an energy device with multi-electron redox reactions [126]. The unique structure and surface functional groups of nanocarbon materials endow them with remarkable abilities to manipulate the electron structures of active components, and therefore optimize the adsorption energy and catalytic activities [125,127,128].

More specifically, to rationally design the nanocarbon-based electrocatalysts with optimized interfacial charge transfer, the structural hybrids at molecular level with alternate stacking or “van der Waals heterostructure” is of great interest [129]. Graphene can be hetero-assembled with other 2D materials, such as exfoliated LDH sheets [130,131] and transition metal dichalcogenides [132]. With an integration of the high conductivity of graphene sheets, highly exposed active centers of 2D nanolayers, facilitated charge transport, and strong synergistic effects between two components, the electrocatalytic performance of pristine active components can be significantly improved. It was reported that in  $MoS_2$ /graphene vertical heterostructures, a built-in electric field was generated with the direction from  $MoS_2$  to graphene due to

the work function difference, thus facilitating the electron transfer and making  $MoS_2$  positively charged [132]. The bandgap at the  $MoS_2$  domain edge was dramatically decreased from  $\sim 2.20$  to  $\sim 0.30$  eV, and led to rather high HER activities. Most recently, Yao’s group fabricated a heterostructured catalyst by coupling exfoliated NiFe LDH nanosheets and defective graphene (NiFe LDH-NS@DG10) as OER/HER bifunctional catalysts for overall water splitting [129]. The defective graphene not only shortened the diffusion distance and provided catalytic active sites for HER, but also served as a powerful substrate to strongly anchor and couple with the exposed transition metal atoms on NiFe LDHs due to highly active defective sites (Fig. 7(a)) [129]. Density functional theory (DFT) calculations clearly revealed the electron redistribution around the defective sites in graphene after being assembled with NiFe LDHs (Fig. 7(b)) [129]. The localized electron accumulation in defective graphene was supposed to facilitate HER catalysis, while the hole accumulation on NiFe LDH nanosheets was beneficial for OER, leading to enhanced HER and OER superior to each components (Fig. 7(b and d)) [129]. Therefore, the utilization of strong chemical and electronic coupling effect in heterostructures affords a promising strategy for the further development of advanced energy electrocatalysts with enhanced performances and even bifunctional activities.

#### 2.4. Generate confinement effects

With respect to the manipulation of electron structures, there is actually another powerful and well-demonstrated strategy, which is encapsulating active nanoparticles within nanocarbon shells, such as CNTs and graphene [133–136]. In these cases, the graphene layers tightly covering nanoparticles can afford comprehensive confinement effects: 1) spatial restriction to hamper the sintering of nanoparticles, 2) significant electronic interaction to modify the property and activity of carbon shells, and 3) physical isolation of embedded nanoparticles from hostile operating conditions, therefore leading to substantially enhanced catalytic activity and durability [137–139].

Bao’s group has reported a series of pioneer researches on the confinement effects in nanocarbon materials on catalysis, extending this concept from CNTs [138] to graphene [134,140], and from thermocatalysis to electrocatalysis [133,138,140]. Generally, nanocarbon encapsulated Fe nanoparticles are recognized as the most promising high-performance non-precious-metal based ORR catalysts in both acid and alkaline [141–143]; however, the underlying reason is not clear. Assisted by theoretical calculation and advanced characterizations, Bao and co-workers revealed the importance of the encapsulating carbon shell and the electronic interaction between core and shell [138]. As shown in Fig. 8(a), a unique composite with Fe nanoparticles encapsulated in pod-like CNTs was employed as a model to study the nature of nanocarbon-confined electrocatalysts [138]. The UV laser enhanced photoemission electron microscopy (PEEM) image showed a significantly bright spot corresponded to the encapsulated Fe nanoparticles in CNTs, suggesting a decreased work function (Fig. 8(b)). DFT calculations further illustrated the electronic interaction between Fe nanoparticles and carbon shells, exhibiting extra features in the low-density of states (DOS) region near Fermi level, a charge transfer from the Fe cluster to SWCNT of 1.45 electrons, a raised Fermi level by 0.5 eV, and an increase of  $P_z$  charge density at the C atoms surrounding the Fe cluster (Fig. 8(c)). The adsorption free energy of  $O_2$  was also remarkably decreased compared with pristine SWCNTs (Fig. 8(d)). In general, the encapsulation-induced confinement effect is demonstrated to decrease the local work function, increase the DOS near Fermi level, and enhance the chemical reactivity of the modified region of the CNT exterior. The resultant electron transfer and performance enhancement have

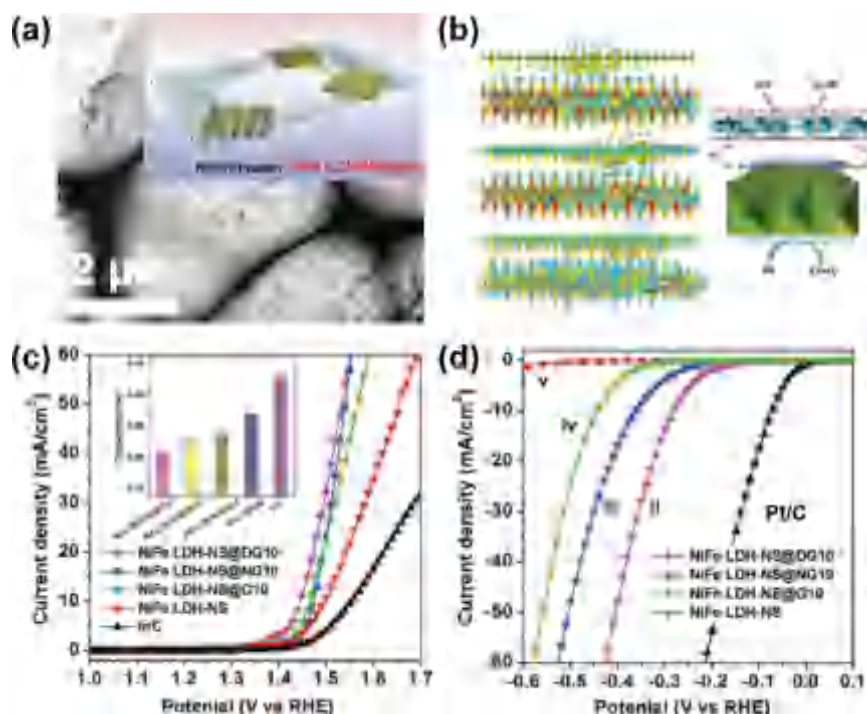


**Fig. 7.** Nanocarbons manipulate the electron structures of both components. (a) TEM image of NiFe LDH-NS@DG10. (b) Calculated 3D charge density difference plots between NiFe LDH and defective graphene (left) and proposed electrocatalytic mechanism (right). (c) OER and (d) HER performances obtained in 1.0 M KOH solution [129].

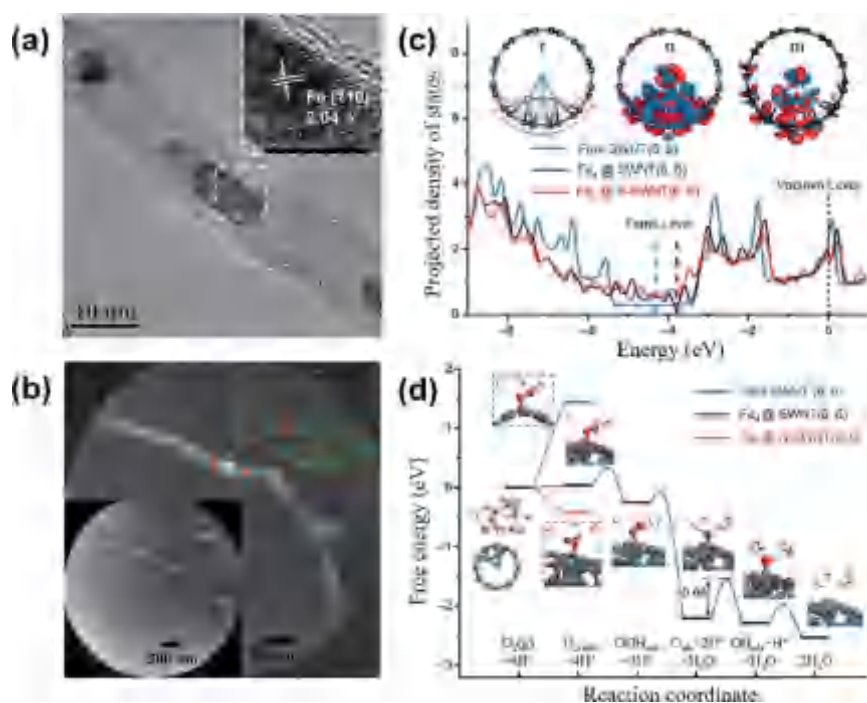


**Fig. 8.** Nanocarbons generate confinement effects. (a) TEM and (b) PEEM images of Fe nanoparticles encapsulated in pod-like CNTs. (c) Calculated projected DOS of the p orbitals of C atoms bonded to different structures. (d) Free-energy diagram of ORR on Fe<sub>4</sub>@SWCNT [138].

been widely revealed in various systems, such as N-doped carbon shell@Fe nanoparticles for ORR [138,142], N-doped CNT@Co nanoparticles for ORR/OER [144,145], N-doped graphene@PtPd alloy for HER/ORR [146], N-enriched mesoporous carbon@CuCo alloy for ORR/HER [147], graphene@FeNi alloy for OER [140], N, O, S tri-doped carbon@Co<sub>9</sub>S<sub>8</sub> for ORR/OER [148], N-doped graphene@ $\gamma$ -Fe<sub>2</sub>O<sub>3</sub> for ORR [149], etc.

Notably, the encapsulating carbon shells were dominantly heteroatom-doped and few-layered, which is essential and

beneficial for the improved activity. It was theoretically revealed that the N doping can further increase the DOS near Fermi level, reduce the work function, and decrease the adsorption free energy of the C atoms surrounding the encapsulate Fe clusters, compared with un-doped graphene encapsulation [138]. On one hand, the N doping is crucial for the formation of Fe-induced active sites. Some research believe that the porphyrin-like FeN<sub>4</sub> (or FeN<sub>x</sub>) structure are the effective active sites for ORR [143,150,151], while some other investigations suggest that the polymeric N species

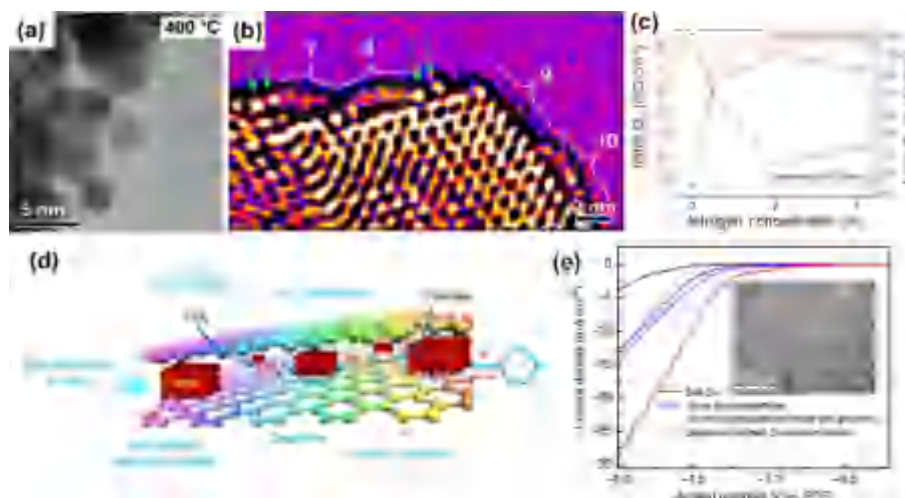


**Fig. 9.** Nanocarbons generate confinement effects. (a) TEM image of the graphene@Pt structure formed without nitrogen precursor. (b) False color view of the aberration corrected TEM image of defective graphene@Pt structure formed with nitrogen precursor (0.5% with ethanol). (c) The initial (after 100 cycles) and final (after 1000 cycles) Coulombic charge for hydrogen desorption for samples with varying nitrogen precursor amounts [139]. (d) Schematic illustration of the graphene confined Sn nanosheets for  $\text{CO}_2$  electroreduction, and (e) the performance obtained in  $\text{CO}_2$ -saturated 0.10 M  $\text{NaHCO}_3$ , with a TEM image inset [154].

promote the nucleation and formation of small superparamagnetic Fe nanoparticles encapsulated in carbon supports, which provide ORR active sites instead of  $\text{FeN}_4$  species [152]. On the other hand, the incorporated nitrogen and other heteroatoms themselves can tune the surface functionality and electrocatalytic activities of the carbon matrix via electron or spin redistribution [140,148,152]. Additionally, the atomic modulation of the encapsulated nanoparticles, especially the formation of bimetal alloys (e.g. FeCo, CuCo, FeNi, etc.), also provides a versatile strategy to facilitate the formation of N-enriched carbon shell, enhance the synergetic coupling, and further boost the electrocatalytic performances compared to mono-metal nanoparticles [137,140,147].

Besides the enhancement of catalytic activity, the nanocarbon encapsulated core-shell nanoparticles always exhibit remarkably improved durability in acid and alkaline mediums as highlighted above [138,142,148,153]. However, the achieved superior resilience to degradation may sacrifice the overall catalyst efficacy in some cases. Taking graphene@Pt nanoparticles for instance, the graphene encapsulated samples were demonstrated to show much better durability without any degradation after 1000 cycles, attributed to the graphene protection from etching, oxidation, and aggregation (Fig. 9(a–c)) [139]. Nevertheless, the complete envelop by a continuous graphene shell would limit the access of reactants to the catalytic Pt surface and inhibit the performance. If porous defects were introduced into the graphene shells by pyridine addition during synthesis (Fig. 9(b)), reactants were able to readily access the Pt surface by permeating through the pores, while the remaining graphene shield still possessed effective protection. Therefore, an optimal compromise between electrocatalytic activity and durability can be achieved by the engineering of the encapsulating graphene shell with favorable coverage and defects (Fig. 9(c)) [139].

The confinement effect can also be rationally extended from 3D core-shell structure to 2D lamellar materials, such as graphene and hexagonal boron nitride, stimulating a new field of “electrochemistry under 2D cover” [134]. The space under the 2D cover can serve as nanocontainers for atoms, molecules, and even solutions, and also nanoreactors for nanomaterial synthesis and confined catalysis. The 2D confinement can modulate the molecule adsorption and tune the reaction activity and selectivity [134]. For instance, Xie and co-workers synthesized a hybrid electrocatalyst of

graphene confined Sn quantum sheets via spatially confined reduction strategy for  $\text{CO}_2$  electroreduction [154]. The unique structure endowed several advantages, including the protection of graphene avoiding the oxidation of active metal in air, increased ECSA ensuring higher  $\text{CO}_2$  adsorption capacity, lowered Sn–Sn coordination number efficiently stabilizing the  $\text{CO}_2^-$  intermediates, and high conductivity facilitating the charge transfer (Fig. 9(d)). Consequently, the Sn quantum sheets confined in graphene showed significantly enhanced electrocatalytic activity and stability for  $\text{CO}_2$  electroreduction compared with Sn nanoparticles or Sn/graphene mixture (Fig. 9(e)) [154].

### 2.5. Support electrocatalysts into 3D free-standing electrodes

Most electrocatalysts are in the form of fine powders and nanoparticles, and tested by drop-casting on glass carbon electrode or nickel foam. Such powdery structure and electrode fabrication procedure result in uncontrolled electrocatalyst distribution with the coffee-ring effect, a plenty of dead volumes, undesirable interfaces due to the use of binders, and peeling of catalysts during the gas evolution. Therefore, aiming at the high activity and durability for practical applications, the development of free-standing self-supported electrocatalysts directly growing on 3D conductive substrates or assembled into 2D flexible films has been strongly considered [155]. Compared with powdery electrocatalysts, the self-supported electrocatalysts not only lead to direct contact and strong adhesion between electroactive species and conductive substrates without binder for better electron transfer and long-term durability, but also possess 3D porous architectures to enhance the utilization of active sites and facilitate the electrolyte penetration [155,156].

Various metal substrates, such as nickel foam [157,158], copper foil [159], and stainless steel mesh [160] are employed to cultivate electroactive components for 3D self-supported electrocatalysts via hydrothermal process or electrodeposition. Although the high conductivity and 3D porous framework of these metal substrates benefit the electrocatalytic reactivity and durability, the rigid and bulky configuration limits the flexibility and versatility of obtained electrodes. As an impressive alternative, the carbon fiber paper is a typical soft current collector with high conductivity, flexibility, and shape conformability [161]. After certain indis-

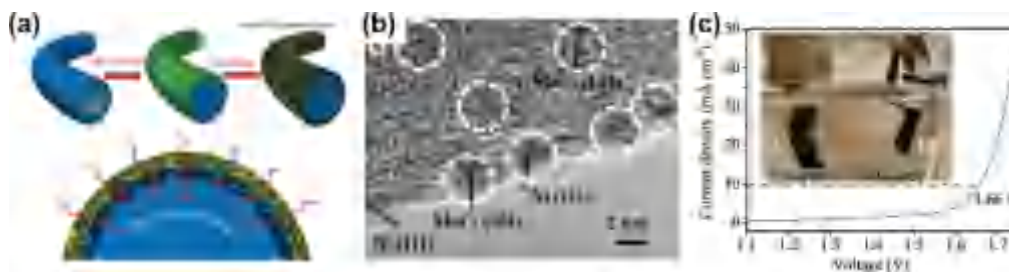


**Fig. 10.** Nanocarbons support electrocatalysts into 3D free-standing electrodes. (a) Scheme and (b) TEM image of metal nanoparticles/N-doped porous carbon hybrids coated on carbon fibers. (c) Overall water splitting based on NiMo-PVP as the HER electrode and NiFe-PVP as the OER electrode in 1.0 M KOH [166].

pensable pretreatment through mild oxidation or oxygen plasma, the carbon fiber paper can serve as favorable substrates to grow various electroactive materials for targeted applications, such as phosphorus-doped  $g\text{-C}_3\text{N}_4$  for ORR/OER [162],  $\text{Mo}_2\text{C}$  micro-islands for HER [163],  $\text{Co}_3\text{O}_4$  nanoparticles for ORR [164], vertical NiCo LDH nanosheets for OER [165], etc. Recently, Zhang and co-workers reported a simple method to successfully fabricate a series of ultrafine metal nanoparticles/N-doped porous carbon film coated on carbon fiber papers (Fig. 10(a)) [166]. The mixed precursor of metal salts and polyvinylpyrrolidone (PVP) was uniformly covered on plasma-cleaned carbon fibers by dip coating, followed by annealing at 1000 °C, during which the *in-situ* reduction of metal precursors and metal-assisted carbon etching process generated nanosized metal particles embedded in N-doped porous carbon (Fig. 10(b)). As-synthesized NiMo-PVP exhibited excellent HER activity with a low overpotential of 130 mV for 10  $\text{mA cm}^{-2}$ , and NiFe-PVP showed outstanding OER performance with a small overpotential of 297 mV for 10  $\text{mA cm}^{-2}$ . These two self-supported electrocatalysts were coupled for overall water splitting, delivering a low potential for a current density of 10  $\text{mA cm}^{-2}$  (1.66 V) and a high Faradic efficiency around 100% (Fig. 10(c)) [166].

The flourishing of nanocarbon affords more opportunities for the controllable construction of self-supported electrocatalysts. For instance, the 2D graphene sheets can be facilely assembled into 3D porous architectures, such as hydrogels, aerogels, foam, and film via chemical vapor deposition, hydrothermal treatment, or vacuum filtration [60,167–171]. With the doping of heteroatoms or decoration of active species, graphene gel-based monolithic materials have been demonstrated as promising catalysts for ORR [167,172], OER [60,173–175], and HER [176,177]. The oxygen-containing functional groups, in-plane pores, or nitrogen dopants in partially reduced/doped graphene oxides are demonstrated to be anchoring sites for active species and facilitating their well dispersion. For instance, two-step heterogeneous reactions were explored to incorporate Ni nanoparticles into nitrogen-doped graphene film (Ni-NG) as an excellent freestanding ORR electrocatalyst (Fig. 11(a)) [168]. The graphene sheets were self-assembled into a lamellar structure in advance and nickel particles were then grown and confined inside (Fig. 11(b)). The residual functional groups on the graphene were dominant in the nucleation of Ni particles and facile formation of such hybrid films. As a result, the unique structure enabled seamless electrode contact (3D conductive framework and well developed porosity) and high catalyst loading (Ni/NiOOH and Ni-O/N-C active sites), leading to favorable electrode kinetics and strong durability (Fig. 11(c)) [168]. Similarly, metal oxides [122] and hydroxides [122] were also deposited on graphene sheets to form efficient self-supported OER catalysts.

Additionally, the facile assembly of freestanding van der Waals heterostructured films with various 2D components has applied as a wide range of self-supported electrocatalysts. Graphene sheets and its analogues (e.g.  $\text{MoS}_2$  [178,179],  $\text{WS}_2$  [180],  $g\text{-C}_3\text{N}_4$  [102], MXene [181], etc.) can be parallelly stacked and orderly assembled into porous films by vacuum filtration of their mixture, in which

commonly one enables the conductive scaffold and the other provides highly electroactive sites. Qiao's group has reported a series of heterostructured electrocatalysts, such as porous  $\text{C}_3\text{N}_4/\text{N}$ -graphene film for HER [182], 3D  $\text{WS}_2/\text{P,N,O}$ -doped graphene film for HER [183], and  $\text{Ti}_3\text{C}_2/g\text{-C}_3\text{N}_4$  film for ORR/OER [103], exhibiting extraordinary performances comparable to precious metal catalysts and robust durability. In the case of  $\text{Ti}_3\text{C}_2/g\text{-C}_3\text{N}_4$  film, the  $\text{Ti}_3\text{C}_2$  possess excellent conductivity and hydrophilic features and  $g\text{-C}_3\text{N}_4$  contains ultrahigh N contents (Fig. 11(d)) [103]. The overlapped assembly and strong couple between  $\text{Ti}_3\text{C}_2$  and  $g\text{-C}_3\text{N}_4$  not only achieved a freestanding film with a porous structure, conductive framework, and hydrophilic surface (Fig. 11(e)), but also generated Ti-N<sub>x</sub> motifs serving as excellent active sites for ORR and OER (Fig. 11(f)). Such high-performance freestanding electrocatalysts were also directly used as the cathodes for rechargeable Zn-air batteries, which largely outperformed those catalyzed by coated powdery  $\text{IrO}_2/\text{C}$  catalyst [103].

As a conclusion for this section, we have classified and discussed several chief functionalities for nanocarbon substrates in hybrid electrocatalysts. However, it is worth noting that the role of the nanocarbon component is always comprehensive and synergistic in every hybrid electrocatalyst. The introduction of active sites is an effective routine to enhance the electrocatalytic performance and boost the potential of electrocatalyst for fuel cells [184–186] and batteries [187–189]. As highlighted above, porous graphene frameworks can be utilized to effectively modify the growth of active components, which is also likely to form strongly coupled interfaces with charge transfer and manipulate electron structures of active sites. Meanwhile, the high conductivity and hierarchical scaffolds benefit the electron and mass transport. Confinement effects can also be generated in specific hybrids, such as core-shell and van der Waals heterostructures. Therefore, the in-depth understanding and rational integration of each functionalities are believed to fully utilize the advantages of nanocarbon substrates in energy electrocatalysis.

### 3. Nanocarbons providing highly active sites

Since the discovery of superb ORR electrocatalytic performances of N-doped CNTs in 2009 [190], tremendous efforts have been devoted to explore the metal-free functionalized nanocarbons toward outstanding activities comparable to precious-metal catalysts for vast catalytic processes. Up to date, various metal-free nanocarbon materials with tunable functionalities and structures have been developed to be effective for ORR, OER, and HER electrocatalysis [191–195], along with which, the insight into the intrinsic activity mechanism has been strongly enhanced [40,196,197]. Both experimentally and theoretically, it is strongly revealed that the charge-transfer or spin-redistribution on  $sp^2$  conjugated carbon matrix induced by heteroatom-doping, molecular-doping, edge sites, and topological defects impart the remarkable electrocatalytic activities to nanocarbon materials [128,196,198]. Some recent reviews have provided excellent overviews of present

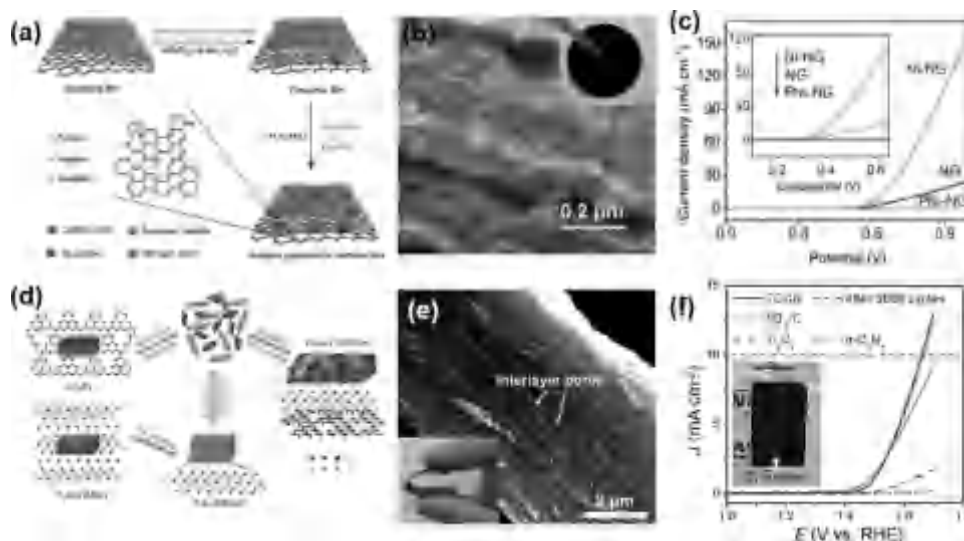


**Fig. 11.** Nanocarbons support electrocatalysts into 3D free-standing film electrodes. (a) Scheme of the fabrication, (b) SEM image, and (c) OER activity of 3D Ni-NG electrode [168]. (d) Scheme of the fabrication, (e) SEM image, and (f) OER activity of  $\text{Ti}_3\text{C}_2/\text{g-C}_3\text{N}_4$  film [103].

achievements and perspectives for future opportunities in the development of nanocarbon-based electrocatalysts [30,31,40,199]. Hence, in this section, we will only focus on several pivotal and rapid-rising directions with respect to the high activity provided by nanocarbons themselves.

### 3.1. Metal-free multi-heteroatom doped nanocarbons

The nitrogen-doping was firstly revealed to be the origin of ORR activities for nanocarbon materials [190], followed by various heteroatom-doped (N, B, S, P, O, etc.) nanocarbons [200–205]. The electronegativity and electron affinity of incorporated heteroatoms are proposed as critical intrinsic material properties determining the catalytic performance [45,206–208]. Besides, the doping configurations and locations can significantly influence the catalytic activities [209–214] and surface pseudoreactions [215,216]. The doping within the distance of edge effect ( $\sim 2.5$  Å) is more beneficial to obtain higher activities compared with the routine basal doping [210]. Additionally, the introduction of the secondary elements to fabricate dual-doped or even tri-doped nanocarbon electrocatalysts is demonstrated to be able to further boost the extraordinary catalytic performances for ORR/OER/HER [192,217].

On one hand, the coexistence of several kinds of heteroatoms can lead to much more active sites than solely doped nanocarbons. For example, in the N, S dual-doped graphene for ORR, the N atoms endow the surrounding C atoms with higher charge density as active sites, while the S atoms affect the spin distribution, making the carbon atoms with higher spin density or S atoms with higher charge density as catalytic centers [218,219]. When N and S were simultaneously doped, the charge/spin densities were increased and the highest spin density was substantially uplifted, leading to higher ORR activity [219]. On the other hand, the synergistic coupling effects between different dopants can considerably enhance the activity of each sites and result in much improved performances. A *h*-BN-free B,N-graphene was proposed and fabricated as a platform to investigate the role of dual doping [220]. N atoms were firstly incorporated into graphene oxide by annealing with  $\text{NH}_3$  at 500 °C, and then B atoms were doped by pyrolysis with  $\text{H}_3\text{BO}_3$  at 900 °C. With this two-step strategy, both B and N were coupled to C without the formation of undesirable *h*-BN phase, proofed by XPS and Fourier transform IR spectra. The B, N co-doped graphene exhibited much higher current

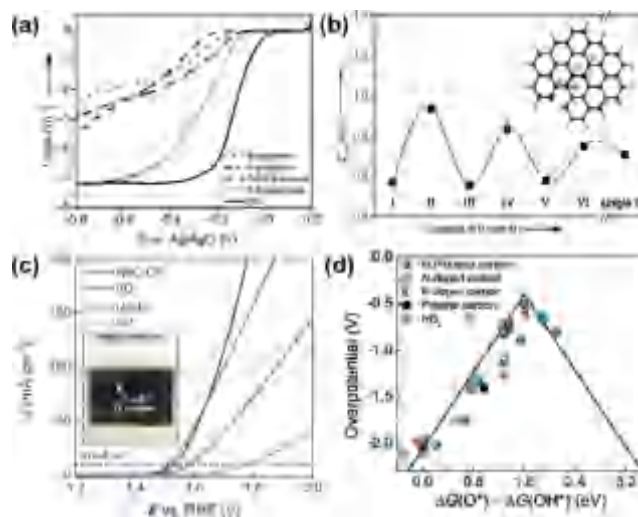


**Fig. 12.** Metal-free multi-heteroatom doped nanocarbons for ORR or OER. (a) ORR performances of various B, N-doped graphene in  $\text{O}_2$ -saturated 0.10 M KOH. (b) Energies of  $\text{HO}_2$  adsorption as a function of the distance between B and N [220]. (c) OER curves of NPC-CP and control samples in  $\text{O}_2$ -saturated 1.0 M KOH. (d) The volcano plot of OER overpotential for different doped nanocarbons [223].

density and more positive onset potential than single-doped samples or *h*-BN/graphene, indicating the synergistic effects (Fig. 12(a)) [220]. DFT calculations revealed that the incorporation of B rendered the less active pyridinic N atoms to be more active, and the electron-withdrawing N atoms indirectly activated B atoms, thus ensuring a higher ORR activity. The distance between two dopants was demonstrated to be critical for the synergistic effect in dual-doped nanocarbon catalysts (Fig. 12(b)) [220].

Multi-heteroatom doped nanocarbon materials are also demonstrated to be more promising for OER catalysis and water splitting. For example, N,O dual-doped carbon hydrogel film [221], N,S dual-doped graphene microwires [222], N,S dual-doped graphite foam [175], and N,P dual-doped carbon nanofibers on carbon paper (NPC-CP) [223] have been proposed as highly active and stable OER catalysts. In the case of NPC-CP, the addition of P dopants was revealed to effectively modify the textural property and porosity resulting in a higher specific surface area of  $473 \text{ m}^2 \text{ g}^{-1}$  [223]. The

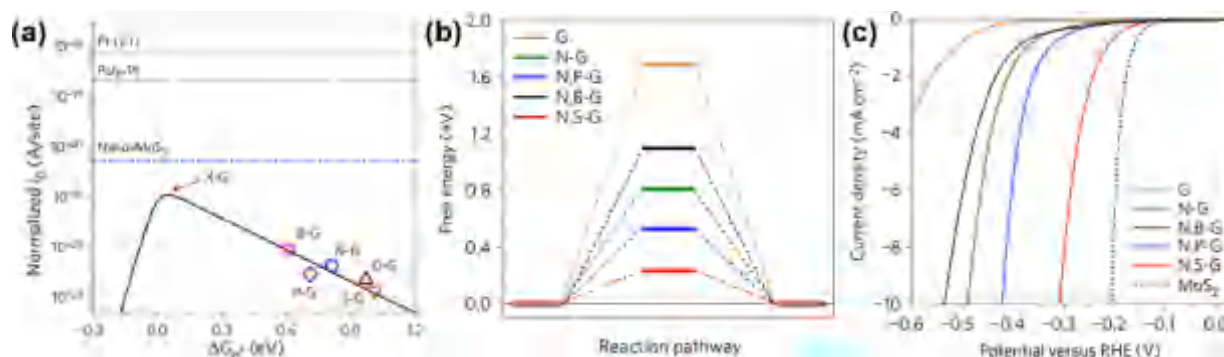


**Fig. 13.** Metal-free multi-heteroatom doped nanocarbons for HER. (a) Volcano plot between the normalized theoretical exchange current per active site and free energy change of hydrogen adsorption. (b) The free energy diagram for graphene with different doping. (c) HER LSV curves obtained in 0.5 M  $\text{H}_2\text{SO}_4$  [192].

free-standing electrocatalyst can be applied as the working electrode for OER directly, which exhibited excellent stability and high activity with a low overpotential of 310 mV required for 10  $\text{mA cm}^{-2}$  (Fig. 12(c)) [223]. Theoretical calculations clearly highlighted the crucial role of dual-doping on OER activity, suggesting a minimum overpotential of 0.505 V achieved for N,P co-doped carbon which was lower than single-doped and pristine carbons and even superior to  $\text{IrO}_2$  (Fig. 12(d)) [223]. Furthermore, the rational design of multi-heteroatom doped nanocarbon materials not only enhances the catalytic activities, but also introduces multifunctional performances, such as N,P dual-doped carbon network [194] and N,S dual-doped carbon tubes [224] with extraordinary activity for ORR and good activity for HER, as well as N,P,F tri-doped graphene [225] and N,S dual-doped porous graphitic sheets [226] as trifunctional catalysts for ORR, OER, and HER.

It is notable that despite the great achievements in metal-free carbon catalysts for ORR/OER, the intrinsic electrocatalytic activity of nanocarbons for HER is still far from satisfactory. In the first report of metal-free HER electrocatalyst, it was revealed that the chemical adsorption of  $\text{H}^*$  is too strong on  $\text{g-C}_3\text{N}_4$ , but too weak on N-graphene, leading to unfavorable HER catalysis [195]. A mediated adsorption-desorption behavior can be achieved by the chemical coupling between  $\text{g-C}_3\text{N}_4$  and N-graphene to facilitate the HER kinetics and improve the performance, comparable to nanostructured  $\text{MoS}_2$  materials [195]. The specific heteroatom doping and strongly coupled interface are able to tune the  $\text{H}^*$  adsorption abilities toward better HER activities. However, further investigations suggested that even climbing to the volcano peak by single-heteroatom-doping, the HER activity of graphene was still largely inferior to Pt/C and  $\text{MoS}_2$  (Fig. 13(a)) due to the weak adsorption of  $\text{H}^*$  on graphene [192]. Inspired by theoretical results, the introduction of secondary heteroatom dopants was proposed as an effective strategy to further modify the electron acceptor-donor properties and adsorption energy of  $\text{H}^*$  with synergistic coupling effects (Fig. 13(b and c)) [192]. As excellent proofs of concept, N, P co-doped [227] and N, S co-doped [192] graphene have been fabricated to serve as highly active metal-free catalysts for HER, considerably improved than the single-doped counterparts. Therefore, the fabrication of multi-heteroatom doped nanocarbon materials with rational combination and configurations is a promising direction to further boost the electrocatalytic performances of nanocarbons with higher activity and even multifunctional electrocatalytic ability.

### 3.2. Hierarchical structure for fully exposed active sites

For metal-free nanocarbon materials, the enrichment of active sites by multi-heteroatom doping and the mixture of doping, edges, or defects are suggested as an effective strategy to

improve the electrocatalytic activities. However, with respect to the apparent overall activity, both the number of intrinsic active sites and the utilization efficiency determined by the accessibility can make a great difference. Therefore, the hierarchical nanostructure of metal-free nanocarbon materials is also of significant importance on the resultant catalytic performances [192,201,228–235].

In the first report of nitrogen-doped CNTs for ORR catalysis [190], the sample with aligned CNTs exhibited much better performance than the non-aligned counterpart, which was attributed to the favorable top-end alignment facilitating the electrolyte/reactant diffusion and accessibility to the active sites on the CNT surface. It was also predicted that if the specific surface area of graphene was increased to  $1000 \text{ m}^2 \text{ g}^{-1}$  at a constant doping level, the overall HER activity can be significantly improved and even better than that of  $\text{MoS}_2$  [192]. Up to date, many well-designed nanostructures have been fabricated to fully expose the active sites and enhance the electrocatalytic activity [182,195,229–231]. As shown in Fig. 14(a), a CNT@NCNT coaxial nanocable was proposed to enrich the nitrogen atoms on surface of CNTs for higher utilization efficiency and enhanced electrocatalytic activity [230]. A thin N-doped turbostratic carbon shell was epitaxially grown on pristine CNTs via the chemical vapor deposition of pyridine (Fig. 14(b)). The N/C ratio on surface was determined to be higher than bulk by XPS analysis and elemental analysis. The ORR activity of CNT@NCNT was revealed to be better than routine N-doped CNTs despite a lower bulk N amount (Fig. 14(c)), indicating the efficient utilization of active sites in such unique nanostructure. The surface of CNTs can be also modified through hydrothermal carbonization in the presence of glucose and urea toward high ORR reactivity [236].

In addition to the 1D coaxial structures with surface-enriched active sites, 2D porous components are also widely employed to fabricate nanocarbon catalysts with high surface area, nanometer thickness, interconnected transport channels, and thereby highly exposed active sites [101,182,219]. For instance, 2D mesoporous  $\text{g-C}_3\text{N}_4$  was *in-situ* grown on 2D mesoporous graphene sheets to form a mesh-on-mesh network (Fig. 14(d)) [101]. In addition to the strong coupling effect between  $\text{g-C}_3\text{N}_4$  and graphene and the multipathway of charge and mass transport, the in-plane mesoporous structure affords much more active sites for hydrogen adsorption, both at the exposed edges and rich defects. As a result, the HER activity was superior to most metal-free catalysts and even better than some non-noble metallic catalysts (Fig. 14(e)) [101].

To synthesize nanocarbon materials with the simultaneous optimization of both surface functionalities and porous structures, effective and scalable strategies are expected, among which the polymerization and subsequent pyrolysis has been demonstrated as a versatile method for various nanocarbon electrocatalysts with high conductivity, large surface area, well-designed porosity, and tunable doping [193,237–240]. For example, the one-step pyrolysis of a polyaniline aerogel template-free polymerized from phytic acid

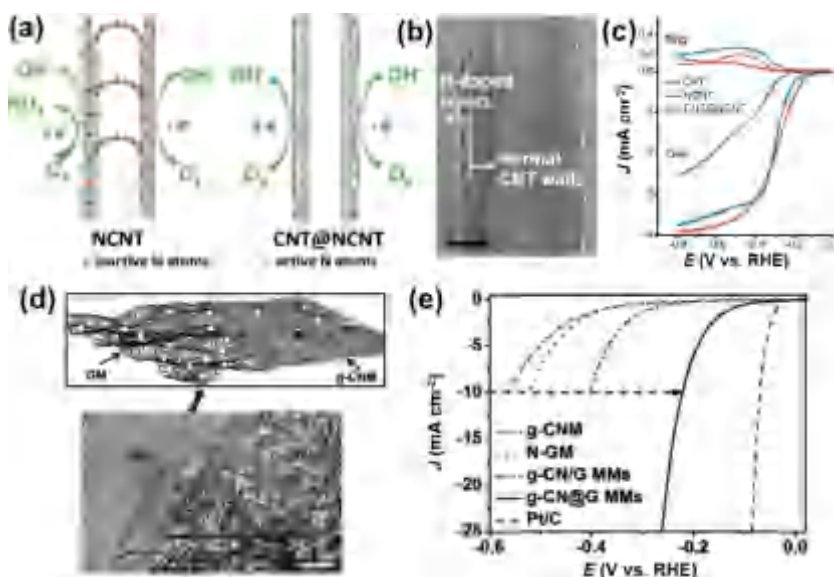


**Fig. 14.** Hierarchical structure for fully exposed active sites. (a) Scheme of the CNT@NCNT structure. (b) TEM image of CNT@NCNT nanocable. (c) ORR LSV curves obtained in  $O_2$ -saturated 0.10 M KOH [230]. (d) Scheme and TEM image of the mesh-on-mesh  $g-C_3N_4$ @graphene hybrid. (e) HER polarization curves of various catalysts obtained in 0.5 M  $H_2SO_4$  [101].

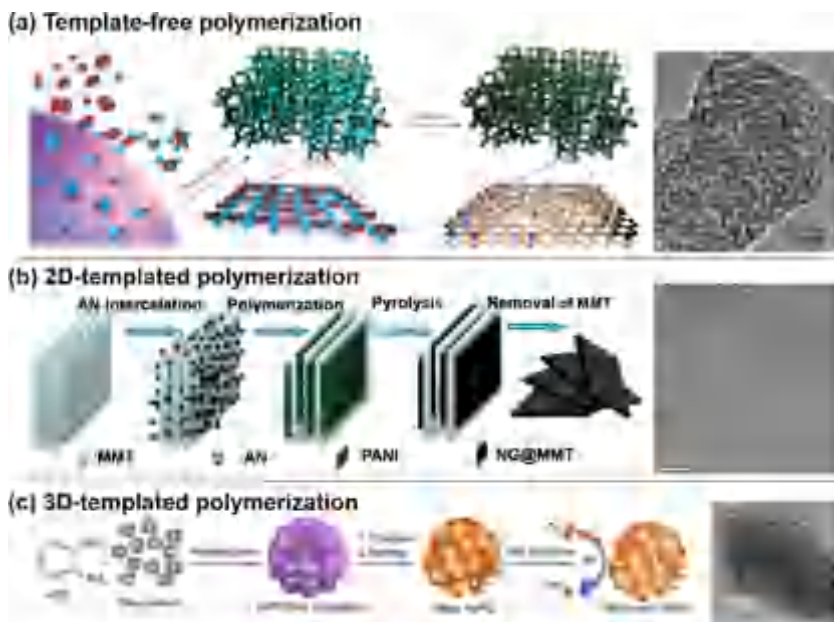


**Fig. 15.** Hierarchical structure for fully exposed active sites synthesized by different methods. (a) Template-free polymerization [193]. (b) 2D-templated polymerization using layered MMT [237]. (c) 3D-templated polymerization using silica colloid [238].

and aniline monomers resulted in mesoporous N,P co-doped carbon foam with a large surface area of  $\sim 1663 \text{ m}^2 \text{ g}^{-1}$  and effective electrocatalytic activities for both ORR and OER (Fig. 15(a)) [193]. With the assistance of 2D layered montmorillonite (MMT) as a quasi-closed flat nanoreactor, the *in-situ* oxidation polymerization of aniline generated nitrogen-doped graphene with a high yield of planar N (90.3% for pyridinic and pyrrolic N) and remarkable ORR activity in acid (Fig. 15(b)) [237]. The spatial confinement effect of MMT (interspace width  $< 1 \text{ nm}$ ) extensively constrained the formation of quaternary N due to its 3D structure. 3D templates such as silica colloid were also employed to manipulate the polymerization of nitrogen-enriched aromatic polymers into nitrogen-doped mesoporous carbons for ORR catalysis [238]. The subsequent  $NH_3$  activation can further modify the porous structure with higher surface area (increased from 685 to  $1280 \text{ m}^2 \text{ g}^{-1}$ ) and meso/micro multi-

modal distribution, leading to substantial improvement in the ORR activity [238]. These results strongly suggest the importance of the hierarchical structure of functionalized nanocarbons for optimizing the electrocatalytic activities, and also afford a series of effective synthetic protocols for the further development.

### 3.3. The role of intrinsic topological defects

The intrinsic topological defects, such as dangling groups, single/multiple vacancies, non-hexagonal topologies, and lattice reconstruction, are always unavoidable in nanocarbon materials, concomitant with the heteroatom-doping and hierarchical structure during synthesis or post-treatment [241,242]. Consequently, a comprehensive understanding of the role of intrinsic topological defects is essentially significant to identify the real active

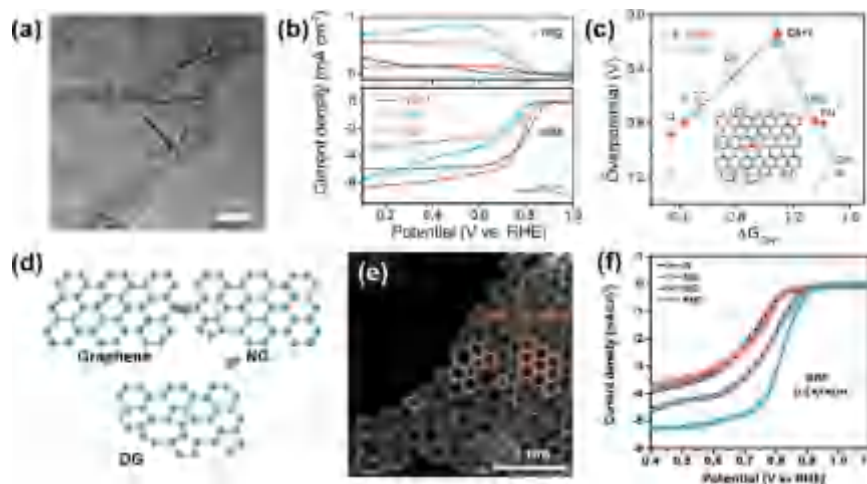


**Fig. 16.** The role of intrinsic topological defects on electrocatalytic activities. (a) TEM image of nitrogen-doped graphene mesh. (b) ORR LSV curves obtained in  $O_2$ -saturated 0.10 M KOH. (c) The volcano plot correlating the overpotential and adsorption of  $OH^*$  [127]. (d) Scheme of the nitrogen removal procedure to make defective graphene without nitrogen (NG). (e) HAADF image of NG. (f) ORR LSV curves for NG, the pristine graphene, and nitrogen-doped graphene [245].

configurations and accelerate the further material innovation, which has been strongly considered recently [127,196,243–249].

As early as 1999, Ajayan and co-workers reported the improved catalytic behavior at CNT electrodes for oxygen reduction, which was ascribed to the pentagons at CNT tips, pentagon–heptagon defect pairs in lattice (Stone–Wales defect), and curvature, by DFT calculations and molecular dynamics simulations [250,251]. The non-hexagonal topological defects can locally induce Gaussian curvatures and thereby regulate the adsorption and reduction of oxygen [252,253]. Furthermore, the influence of different types of point/line defects in graphene on ORR catalytic properties was investigated by DFT calculations [254]. It was revealed that some specific defects, such as a pentagon carbon ring at zigzag edge or pentagon–pentagon–octagon chains can induce local charge and spin polarization, which were mainly located at the zigzag edges or some defects themselves and suggested to be catalytically active [254]. Recently, several metal-free and dopant-free nanocarbon materials were fabricated via metal-/heteroatom-free growth or post-treatment to convincingly reveal the intrinsic activity of topological defects [127,243,246,247,255]. Specifically, the pentagon [243,245], zigzag edge [243], and different combinations (e.g. 57 [127], 585 [245], 7557 [245]) have been confirmed as effective active sites for ORR both experimentally and theoretically, and even promising for OER and HER. A defect-rich graphene mesh was fabricated by MgO-templated carbonization with tunable nitrogen doping and porosity (Fig. 16(a and b)) [127]. The electrocatalytic activity of different species was demonstrated in the order: topological defects > doping at edge > doping in bulk, with a nitrogen-free topological defect (57 defect) at the peak of volcano plots for both ORR and OER (Fig. 16(b and c)). In addition to the material synthesis, performance test and DFT calculation, advanced characterizations such as aberration-corrected high-resolution TEM was also used to visualize the topological defects in graphene and proof the importance of intrinsic defects more clearly (Fig. 16(d–f)) [245].

The topological defects in nanocarbon materials, especially the defects in porous graphene, can not only serve as highly active catalytic centers, but also benefit the fabrication of novel nanostructured catalysts. As shown in Fig. 7, the defective graphene can be employed as effective substrates to strongly anchor and chemically/electronically couple with NiFe LDHs, leading to enhanced OER/HER activities [129]. For another promising active sites, the metal–nitrogen–carbon species were theoretically revealed to be more energetically feasible at graphitic edges (Fig. 17(a)) [256],

suggesting new synthetic methodologies to controllably fabricate catalysts at atomic precision via defect engineering [112]. Co, N, O tri-doped graphene catalyst with atomically dispersed Co– $N_x$ –C active sites was facilely fabricated with the assistance of abundant defective graphene edges for the anchor of Co species (Fig. 17(b–d)). After acid treatment, no obvious nanoparticle was obtained in TEM images, and the bulk Co content was detected to be as low as 1.23 wt%. XPS characterization indicated the presence of Co– $N_x$ –C (399.3 eV) by bonding pyridinic N to Co, with ca. 1 eV up-shift from pristine pyridinic N (~398.4 eV). The present of Co– $N_x$ –C active sites further enhanced the ORR/OER activity of graphene with nitrogen dopants and topological defects (50 mV more positive half-wave potential), and exhibited promising application in rechargeable Zn–air batteries [112].

To summarize up this section, nanocarbon materials have been widely demonstrated to exhibit remarkable intrinsic electrocatalytic activities for ORR, OER, HER, and other electrocatalysis. With optimized surface characterizations (e.g. doping, edges, defects, functional groups) and appropriate multiscale hierarchy (e.g. higher surface area, micro/meso porosity) [31,40,43,192], the performance of metal-free nanocarbon materials is further enhanced and potentially overtakes metal-based counterparts. For fundamental investigation, it is notable that many possible effects (e.g. metal impurities, combination of various active sites) should be concerned to afford more rigorous and convincing insight of the activity mechanism for nanocarbon materials. However, the uniformity of material synthesis and the durability of nanocarbon during operation conditions deserve more attention toward practical applications in energy electrocatalysis.

#### 4. Conclusions and perspectives

During the last decade, the application of nanocarbon materials in the field of energy electrocatalysis has witnessed exciting achievements. Contributed to the unique features of nanocarbon materials, they can serve as multifunctional substrates or provide highly active sites for excellent performances in ORR, OER, HER,  $CO_2$  reduction, and so on. Nanocarbons with appropriate structures and functionalities are employed to accelerate the electron and mass transport and generate confinement effects. The strongly coupled interface between nanocarbon and the active components will lead to modified incorporation and manipulated electron structures. These effects of the nanocarbon substrate can significantly improve the activity of the pristine active components and

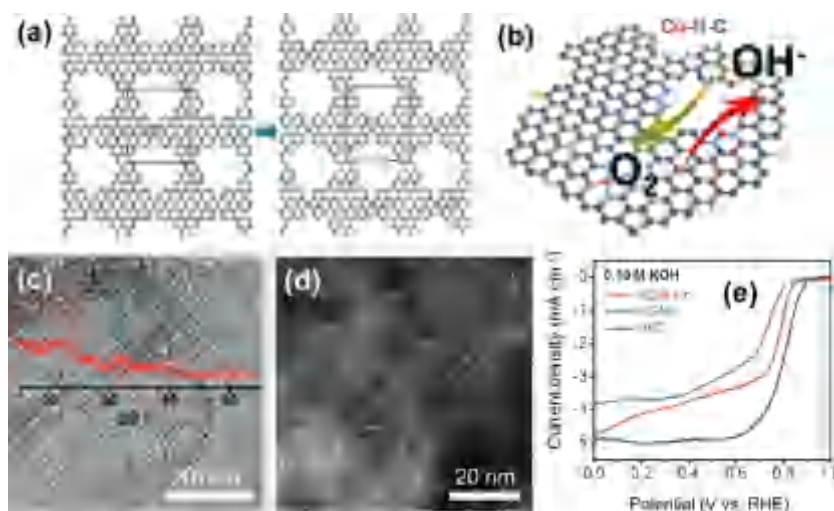


**Fig. 17.** The role of intrinsic topological defects on material synthesis. (a) Atomistic structures of graphitic pores, and metal-N<sub>4</sub> clusters embedded at edge [256]. (b) Scheme of the Co, N, O tri-doped graphene (NGM-Co) for ORR/OER. (c) TEM image of NGM-Co with XRD pattern inset. (d) Dark-field high-resolution TEM image of NGM-Co. (e) ORR LSV curves in O<sub>2</sub>-saturated 0.10 M KOH [112].

enhance the durability. Additionally, the various defective sites in nanocarbons endow themselves with remarkable intrinsic activities even without metal-based components. Several strategies are promising to further accelerate the electrocatalysis, such as the multi-heteroatom doping, hierarchical structure for fully exposed active sites, and the utilization of intrinsic topological defects. Consequently, the performance of nanocarbon-based catalysts has been demonstrated to be greatly improved and even competitive with precious-metal-based catalysts or other benchmark catalysts in some energy technologies, including Zn-air batteries, fuel cells, and water splitting, over the past few years.

Aiming at a thorough understanding of the activity mechanism and practical applications in commercial devices, there are still grand challenges to be dealt with in the field of nanocarbon-based energy electrocatalysts. A combination of new synthetic strategies, advanced characterization, and improved theoretical approach is expected to profoundly and precisely elucidate the activity of specific active sites. Additionally, the relationship between different active sites, hierarchical porosity, hybridization structures, and electrocatalytic performance should be made clear from tremendous reports, in order to guide the material design and efficient development of highly desirable nanocarbon-based catalysts for specific reactions. Furthermore, toward a methodical research and targeted development, the critical evaluation indicators and standard protocols for the test of activity and durability, and also the performance in practical devices, are urgently required to be established. Besides, cost-effective and process-simple large-scale production of nanocarbon materials with well-controlled structure and surface chemistry, and desirable uniformity as well, is essential on the way to industrial applications. With continuous research in this promising field, we believe that the fundamental understanding and practical performance of nanocarbon-based energy electrocatalysts will be impressively improved, which will play an indispensable and prominent role in the future energy scenario.

## Acknowledgments

This work was supported by the National Key Research and Development Program (Nos. 2016YFA0202500 and 2016YFA0200102), the Natural Scientific Foundation of China (No. 21561130151), and Royal Society for the award of a Newton Advanced Fellowship (Ref: NA140249).

## References

- [1] S. Chu, A. Majumdar, *Nature* 488 (2012) 294–303.
- [2] B. Dunn, H. Kamath, J.M. Tarascon, *Science* 334 (2011) 928–935.
- [3] M.K. Debe, *Nature* 486 (2012) 43–51.
- [4] S. Wang, S.P. Jiang, *Natl. Sci. Rev.* 4 (2017) 163–166.
- [5] J.Z. Su, J.L. Zhou, L. Wang, C. Liu, Y.B. Chen, *Sci. Bull.* 62 (2017) 633–644.
- [6] Q. Wang, H.J. Chen, G. Liu, L.Z. Wang, *Sci. Bull.* 60 (2015) 405–418.
- [7] H.-J. Peng, X.-B. Cheng, J.-Q. Huang, Q. Zhang, *Adv. Energy Mater.* 7 (2017) 1700260.
- [8] Y.C. Tu, D.H. Deng, X.H. Bao, *J. Energy Chem.* 25 (2016) 957–966.
- [9] W. Lv, Z.J. Li, Y.Q. Deng, Q.H. Yang, F.Y. Kang, *Energy Storage Mater.* 2 (2016) 107–138.
- [10] P. Zhang, M. Fujitsuka, T. Majima, *J. Energy Chem.* 25 (2016) 917–926.
- [11] Y.M. He, J.E. Thorne, C.H. Wu, P.Y. Ma, C. Du, Q. Dong, J.H. Guo, D.W. Wang, *Chem* 1 (2016) 640–655.
- [12] V. Strauss, A. Roth, M. Sekita, D.M. Guldi, *Chem* 1 (2016) 531–556.
- [13] Y. Li, X.G. Wang, S.M. Dong, X. Chen, G.L. Cui, *Adv. Energy Mater.* 6 (2016) 1600751.
- [14] J. Fu, Z.P. Cano, M.G. Park, A.P. Yu, M. Fowler, Z.W. Chen, *Adv. Mater.* 29 (2017) 1604685.
- [15] J.Y. Xiong, C. Han, Z. Li, S.X. Dou, *Sci. Bull.* 60 (2015) 2083–2090.
- [16] X.Q. Zhang, X.B. Cheng, Q. Zhang, *J. Energy Chem.* 25 (2016) 967–984.
- [17] Z.-F. Huang, J. Wang, Y. Peng, C.-Y. Jung, A. Fisher, X. Wang, *Adv. Energy Mater.* 7 (2017) 1700544.
- [18] H.C. Yang, J. Liang, Z.X. Wang, B.G. An, F. Li, *New Carbon Mater.* 31 (2016) 243–263.
- [19] G.X. Zhang, X.Y. Jin, H.Y. Li, L. Wang, C.J. Hu, X.M. Sun, *Sci. China Mater.* 59 (2016) 337–347.
- [20] K.Q. Lu, Q. Quan, N. Zhang, Y.J. Xu, *J. Energy Chem.* 25 (2016) 927–935.
- [21] W. Zhang, W.Z. Lai, R. Cao, *Chem. Rev.* 117 (2017) 3717–3797.
- [22] S.Q. Lu, Z.B. Zhuang, *Sci. China Mater.* 59 (2016) 217–238.
- [23] J. Liu, C. Guo, A. Vasileff, S. Qiao, *Small Methods* 1 (2017) 1600006.
- [24] L. Zhang, S. Hu, X. Zhu, W. Yang, *J. Energy Chem.* 26 (2017) 593–601.
- [25] R. Liu, C. Stephani, K.L. Tan, D.W. Wang, *Sci. China Mater.* 58 (2015) 515–520.
- [26] S. Abate, G. Centi, P. Lanzafame, S. Perathoner, *J. Energy Chem.* 24 (2015) 535–547.
- [27] D.S. Su, G. Centi, *J. Energy Chem.* 22 (2013) 151–173.
- [28] H.L. Wang, H.J. Dai, *Chem. Soc. Rev.* 42 (2013) 3088–3113.
- [29] C. Tang, H.F. Wang, X.L. Zhu, B.Q. Li, Q. Zhang, *Part. Part. Syst. Charact.* 33 (2016) 473–486.
- [30] C.G. Hu, L.M. Dai, *Angew. Chem. Int. Ed.* 55 (2016) 11736–11758.
- [31] X. Liu, L. Dai, *Nat. Rev. Mater.* 1 (2016) 16064.
- [32] S. Abate, K. Barbera, G. Centi, G. Giorgianni, S. Perathoner, *J. Energy Chem.* 25 (2016) 297–305.
- [33] S. Chung, M. Choun, B. Jeong, J.K. Lee, J. Lee, *J. Energy Chem.* 25 (2016) 258–264.
- [34] C.M. Wang, S. Bai, Y.J. Xiong, *Chin. J. Catal.* 36 (2015) 1476–1493.
- [35] M.L. Dou, M. Hou, Z.L. Li, F. Wang, D. Liang, Z.G. Shao, B.L. Yi, *J. Energy Chem.* 24 (2015) 39–44.
- [36] G.R. Zhang, B.J.M. Etzold, *J. Energy Chem.* 25 (2016) 199–207.
- [37] Y.Y. Gui, Y.L. Cao, G.R. Li, X.P. Ai, X.P. Gao, H.X. Yang, *Energy Storage Mater.* 5 (2016) 165–170.
- [38] Q. Li, T.Y. Wang, D. Havas, H.G. Zhang, P. Xu, J.T. Han, J. Cho, G. Wu, *Adv. Sci.* 3 (2016) 1600140.

- [39] Y.-J. Wang, N. Zhao, B. Fang, H. Li, X.T. Bi, H. Wang, *Chem. Rev.* 115 (2015) 3433–3467.
- [40] C. Tang, Q. Zhang, *Adv. Mater.* 29 (2017) 1604103.
- [41] M. Zhou, H.-L. Wang, S. Guo, *Chem. Soc. Rev.* 45 (2016) 1273–1307.
- [42] M. Gong, H. Dai, *Nano Res.* 8 (2015) 23–39.
- [43] Y.P. Zhu, C.X. Guo, Y. Zheng, S.Z. Qiao, *Acc. Chem. Res.* 50 (2017) 915–923.
- [44] Y. Zheng, Y. Jiao, S.Z. Qiao, *Adv. Mater.* 27 (2015) 5372–5378.
- [45] Z. Zhao, M. Li, L. Zhang, L. Dai, X. Xia, *Adv. Mater.* 27 (2015) 6834–6840.
- [46] Z.L. Wang, D. Xu, J.J. Xu, X.B. Zhang, *Chem. Soc. Rev.* 43 (2014) 7746–7786.
- [47] Y. Jiao, Y. Zheng, M.T. Jaroniec, S.Z. Qiao, *Chem. Soc. Rev.* 44 (2015) 2060–2086.
- [48] Q. Zhang, J.Q. Huang, W.Z. Qian, Y.Y. Zhang, F. Wei, *Small* 9 (2013) 1237–1265.
- [49] J. Liang, Z.H. Sun, F. Li, H.M. Cheng, *Energy Storage Mater.* 2 (2016) 76–106.
- [50] Y.Y. Liang, Y.G. Li, H.L. Wang, J.G. Zhou, J. Wang, T. Regier, H.J. Dai, *Nat. Mater.* 10 (2011) 780–786.
- [51] M. Gong, Y. Li, H. Wang, Y. Liang, J.Z. Wu, J. Zhou, J. Wang, T. Regier, F. Wei, H. Dai, *J. Am. Chem. Soc.* 135 (2013) 8452–8455.
- [52] H.-J. Peng, T.-Z. Hou, Q. Zhang, J.-Q. Huang, X.-B. Cheng, M.-Q. Guo, Z. Yuan, L.-Y. He, F. Wei, *Adv. Mater. Interfaces* 1 (2014) 1400227.
- [53] T.-Z. Hou, W.-T. Xu, X. Chen, H.-J. Peng, J.-Q. Huang, Q. Zhang, *Angew. Chem. Int. Ed.* 56 (2017) 8178–8182.
- [54] D. Tang, J. Liu, X. Wu, R. Liu, X. Han, Y. Han, H. Huang, Y. Liu, Z. Kang, *ACS Appl. Mater. Interfaces* 6 (2014) 7918–7925.
- [55] D.H. Youn, Y. Bin Park, J.Y. Kim, G. Magesh, Y.J. Jang, J.S. Lee, *J. Power Sources* 294 (2015) 437–443.
- [56] R. Chen, G.Z. Sun, C.J. Yang, L.P. Zhang, J.W. Miao, H.B. Tao, H.B. Yang, J.Z. Chen, P. Chen, B. Liu, *Nanoscale Horiz.* 1 (2016) 156–160.
- [57] C. Tang, H.S. Wang, H.F. Wang, Q. Zhang, G.L. Tian, J.Q. Nie, F. Wei, *Adv. Mater.* 27 (2015) 4516–4522.
- [58] Y. Gao, F. Wu, H. Chen, *J. Energy Chem.* 26 (2017) 428–432.
- [59] V.M. Bau, X.J. Bo, L.P. Guo, *J. Energy Chem.* 26 (2017) 63–71.
- [60] S. Chen, J.J. Duan, M. Jaroniec, S.Z. Qiao, *Angew. Chem. Int. Ed.* 52 (2013) 13567–13570.
- [61] A. Kongkanand, K. Vinodgopal, S. Kuwabata, P.V. Kamat, *J. Phys. Chem. B* 110 (2006) 16185–16188.
- [62] L.R. Nan, W.B. Yue, Y. Jiang, *J. Mater. Chem. A* 3 (2015) 22170–22175.
- [63] B.-Q. Li, C. Tang, H.-F. Wang, X.L. Zhu, Q. Zhang, *Sci. Adv.* 2 (2016) e1600495.
- [64] H.-F. Wang, C. Tang, X.L. Zhu, Q. Zhang, *J. Mater. Chem. A* 4 (2016) 3379–3385.
- [65] Z. Dong, T. Wang, J. Zhao, T. Fu, L. Wang, J.L. Li, W.P. Ding, *J. Energy Chem.* 25 (2016) 1021–1026.
- [66] L.Z. Yuan, Z. Yan, L.H. Jiang, E.D. Wang, S.L. Wang, G.Q. Sun, *J. Energy Chem.* 25 (2016) 805–810.
- [67] J. Yu, G. Chen, J. Sunarso, Y.L. Zhu, R. Ran, Z.H. Zhu, W. Zhou, Z.P. Shao, *Adv. Sci.* 3 (2016) 1600060.
- [68] X.Y. Zhou, F. Chen, J. Yang, *J. Energy Chem.* 24 (2015) 448–455.
- [69] Y.M. Sun, G.Y. Zheng, Z.W. Seh, N. Liu, S. Wang, J. Sun, H.R. Lee, Y. Cui, *Chem* 1 (2016) 287–297.
- [70] Z.W. Tang, F. Xu, Y.R. Liang, D.C. Wu, R.W. Fu, *New Carbon Mater.* 30 (2015) 319–326.
- [71] W.W. Wen, M.Z. Zou, Q. Feng, J.X. Li, H. Lai, Z.G. Huang, *J. Energy Chem.* 25 (2016) 445–449.
- [72] J.J. Zhang, A.S. Yu, *Sci. Bull.* 60 (2015) 823–838.
- [73] O. Gerber, S. Begin-Colin, B.P. Pichon, E. Barraud, S. Lemonnier, C. Pham-Huu, B. Daffos, P. Simon, J. Come, D. Begin, *J. Energy Chem.* 25 (2016) 272–277.
- [74] F.L. Lou, D. Chen, *J. Energy Chem.* 24 (2015) 559–586.
- [75] S.L. Candelaria, G.Z. Cao, *Sci. Bull.* 60 (2015) 1587–1597.
- [76] L.J. Xie, G.H. Sun, L.F. Xie, F.Y. Su, X.M. Li, Z. Liu, Q.Q. Kong, C.X. Lu, K.X. Li, C.M. Chen, *New Carbon Mater.* 31 (2016) 37–45.
- [77] M.C. Liu, J.J. Li, W. Han, L. Kang, *J. Energy Chem.* 25 (2016) 601–608.
- [78] Q.L. Zhu, Q. Xu, *Chem* 1 (2016) 220–245.
- [79] N. Seselj, C. Engelbrekt, J.D. Zhang, *Sci. Bull.* 60 (2015) 864–876.
- [80] C.W. Zhang, L.B. Xu, J.F. Chen, *Chin. Chem. Lett.* 27 (2016) 832–836.
- [81] C.F. Zhang, D.M. Tang, X.K. Hu, X.Z. Liu, T. Zhang, H.S. Zhou, *Energy Storage Mater.* 2 (2016) 8–13.
- [82] K.P. Xie, W. Xia, J. Masa, F. Yang, P. Weide, W. Schuhmann, M. Muhler, *J. Energy Chem.* 25 (2016) 282–288.
- [83] Y.B. Huang, M. Zhang, P. Liu, F.L. Cheng, L.S. Wang, *Chin. J. Catal.* 37 (2016) 1249–1256.
- [84] Y.W. Ju, S. Yoo, C. Kim, S. Kim, I.Y. Jeon, J. Shin, J.B. Baek, G. Kim, *Adv. Sci.* 3 (2016) 1500205.
- [85] C. Tang, H.-F. Wang, H.-S. Wang, F. Wei, Q. Zhang, *J. Mater. Chem. A* 4 (2016) 3210–3216.
- [86] X.L. Zhu, C. Tang, H.F. Wang, Q. Zhang, C.H. Yang, F. Wei, *J. Mater. Chem. A* 3 (2015) 24540–24546.
- [87] H.-F. Wang, C. Tang, B. Wang, B.-Q. Li, Q. Zhang, *Adv. Mater.* 29 (2017) 1702327.
- [88] X. Zhang, Z. Wu, X. Zhang, L. Li, Y. Li, H. Xu, X. Li, X. Yu, Z. Zhang, Y. Liang, H. Wang, *Nat. Commun.* 8 (2017) 14675.
- [89] M.H. Shao, Q.W. Chang, J.P. Dodelet, R. Chenitz, *Chem. Rev.* 116 (2016) 3594–3657.
- [90] X. Zhong, L. Wang, H. Zhou, Y.Y. Qin, W.L. Xu, Y. Jiang, Y.Y. Sun, Z.Q. Shi, G.L. Zhuang, X.N. Li, D.H. Mei, J.G. Wang, *Adv. Mater. Interfaces* 2 (2015) 1500365.
- [91] Q.Q. Fu, H.H. Li, S.Y. Ma, B.C. Hu, S.H. Yu, *Sci. China Mater.* 59 (2016) 112–121.
- [92] J. Qi, W. Zhang, R.J. Xiang, K.Q. Liu, H.Y. Wang, M.X. Chen, Y.Z. Han, R. Cao, *Adv. Sci.* 2 (2015) 1500199.
- [93] S. Chen, L.W. Wang, Q. Wu, X. Li, Y. Zhao, H.W. Lai, L.J. Yang, T. Sun, Y. Li, X.Z. Wang, Z. Hu, *Sci. China Chem.* 58 (2015) 180–186.
- [94] Y.P. Liu, G.T. Yu, G.D. Li, Y.H. Sun, T. Asefa, W. Chen, X.X. Zou, *Angew. Chem. Int. Ed.* 54 (2015) 10752–10757.
- [95] J. Yang, G.X. Zhu, Y.J. Liu, J.X. Xia, Z.Y. Ji, X.P. Shen, S.K. Wu, *Adv. Funct. Mater.* 26 (2016) 4712–4721.
- [96] M.F. Shao, R.K. Zhang, Z.H. Li, M. Wei, D.G. Evans, X. Duan, *Chem. Commun.* 51 (2015) 15880–15893.
- [97] L.H. Zhuang, L. Ge, Y.S. Yang, M.R. Li, Y. Jia, X.D. Yao, Z.H. Zhu, *Adv. Mater.* 29 (2017) 1606793.
- [98] R. Liu, Y. Wang, D. Liu, Y. Zou, S. Wang, *Adv. Mater.* 29 (2017) 1701546.
- [99] S. Wan, J. Qi, W. Zhang, W. Wang, S. Zhang, K. Liu, H. Zheng, J. Sun, S. Wang, R. Cao, *Adv. Mater.* 29 (2017) 1700286.
- [100] B.-Q. Li, S.-Y. Zhang, C. Tang, X. Cui, Q. Zhang, *Small* 13 (2017) 1700610.
- [101] Q. Han, Z.H. Cheng, J. Gao, Y. Zhao, Z.P. Zhang, L.M. Dai, L.T. Qu, *Adv. Funct. Mater.* 27 (2017) 1606352.
- [102] Q.H. Liang, Z. Li, X.L. Yu, Z.H. Huang, F.Y. Kang, Q.H. Yang, *Adv. Mater.* 27 (2015) 4634–4639.
- [103] T.Y. Ma, J.L. Cao, M. Jaroniec, S.Z. Qiao, *Angew. Chem. Int. Ed.* 55 (2015) 1138–1142.
- [104] Y. Zhao, Z.X. Song, X. Li, Q. Sun, N.C. Cheng, S. Lawes, X.L. Sun, *Energy Storage Mater.* 2 (2016) 35–62.
- [105] Z.H. Xiang, Q.B. Dai, J.F. Chen, L.M. Dai, *Adv. Mater.* 28 (2016) 6253–6261.
- [106] Z. Xie, Y.-S. Li, L. Chen, D.-L. Jiang, *Acta Polym. Sin.* (12) (2016) 1621–1634.
- [107] T. He, X. Wang, H. Wu, H. Xue, P. Xue, J. Ma, M. Tan, S. He, R. Shen, L. Yi, Y. Zhang, J. Xiang, *ACS Appl. Mater. Interfaces* 9 (2017) 22490–22501.
- [108] R.N. Li, D.T. Zhang, Y.Y. Zhou, X.Y. Wang, G.S. Guo, *Sci. China Chem.* 59 (2016) 746–751.
- [109] X.F. Yang, A.Q. Wang, B.T. Qiao, J. Li, J.Y. Liu, T. Zhang, *Acc. Chem. Res.* 46 (2013) 1740–1748.
- [110] C. Zhu, S. Fu, Q. Shi, D. Du, Y. Lin, *Angew. Chem. Int. Ed.* (2017), doi:10.1002/anie.201703864.
- [111] Y. Zheng, Y. Jiao, Y.H. Zhu, Q.R. Cai, A. Vasileff, L.H. Li, Y. Han, Y. Chen, S.Z. Qiao, *J. Am. Chem. Soc.* 139 (2017) 3336–3339.
- [112] C. Tang, B. Wang, H.-F. Wang, Q. Zhang, *Adv. Mater.* 29 (2017) 1703185.
- [113] P.Z. Chen, T.P. Zhou, L.L. Xing, K. Xu, Y. Tong, H. Xie, L.D. Zhang, W.S. Yan, W.S. Chen, C.Z. Wu, Y. Xie, *Angew. Chem. Int. Ed.* 56 (2017) 610–614.
- [114] Y.J. Chen, S.F. Ji, Y.G. Wang, J.C. Dong, W.X. Chen, Z. Li, R.A. Shen, L.R. Zheng, Z.B. Zhuang, D.S. Wang, Y.D. Li, *Angew. Chem. Int. Ed.* 56 (2017) 6937–6941.
- [115] H.L. Tang, S.C. Cai, S.L. Xie, Z.B. Wang, Y.X. Tong, M. Pan, X.H. Lu, *Adv. Sci.* 3 (2016) 1500265.
- [116] Y. Ye, F. Cai, C. Yan, Y. Li, G. Wang, X. Bao, *J. Energy Chem.* 26 (2017), doi:10.1016/j.jechem.2017.1006.1013.
- [117] Q. Li, H.Y. Pan, D. Higgins, R.G. Cao, G.Q. Zhang, H.F. Lv, K.B. Wu, J. Cho, G. Wu, *Small* 11 (2015) 1443–1452.
- [118] Z.H. Li, M.F. Shao, L. Zhou, R.K. Zhang, C. Zhang, M. Wei, D.G. Evans, X. Duan, *Adv. Mater.* 28 (2016) 2337–2344.
- [119] P. He, X.-Y. Yu, X.W. Lou, *Angew. Chem. Int. Ed.* 56 (2017) 3897–3900.
- [120] B.Y. Guan, L. Yu, X.W. Lou, *Adv. Sci.* 4 (2017) 1700247.
- [121] X.M. Xu, C. Su, W. Zhou, Y.L. Zhu, Y.B. Chen, Z.P. Shao, *Adv. Sci.* 3 (2016) 1500187.
- [122] Y. Peng, B.Z. Lu, N. Wang, L.G. Li, S.W. Chen, *Phys. Chem. Chem. Phys.* 19 (2017) 9336–9348.
- [123] X.M. Ning, Y.H. Li, B.Q. Dong, H.J. Wang, H. Yu, F. Peng, Y.H. Yang, *J. Catal.* 348 (2017) 100–109.
- [124] H. Jin, H. Huang, Y. He, X. Feng, S. Wang, L. Dai, J. Wang, *J. Am. Chem. Soc.* 137 (2015) 7588–7591.
- [125] T.-Z. Hou, X. Chen, H.-J. Peng, J.-Q. Huang, B.-Q. Li, Q. Zhang, B. Li, *Small* 12 (2016) 3283–3291.
- [126] H.J. Peng, Z.W. Zhang, J.Q. Huang, G. Zhang, J. Xie, W.T. Xu, J.L. Shi, X. Chen, X.B. Cheng, Q. Zhang, *Adv. Mater.* 28 (2016) 9551–9558.
- [127] C. Tang, H.-F. Wang, X. Chen, B.-Q. Li, T.-Z. Hou, B. Zhang, Q. Zhang, M.-M. Titirici, F. Wei, *Adv. Mater.* 28 (2016) 6845–6851.
- [128] H.B. Yang, J.W. Miao, S.F. Hung, J.Z. Chen, H.B. Tao, X.Z. Wang, L.P. Zhang, R. Chen, J.J. Gao, H.M. Chen, L.M. Dai, B. Liu, *Sci. Adv.* 2 (2016) e1501122.
- [129] Y. Jia, L.Z. Zhang, G.P. Gao, H. Chen, B. Wang, J.Z. Zhou, M.T. Soo, M. Hong, X.C. Yan, G.R. Qian, J. Zou, A.J. Du, X.D. Yao, *Adv. Mater.* 29 (2017) 1700017.
- [130] W. Ma, R. Ma, C. Wang, J. Liang, X. Liu, K. Zhou, T. Sasaki, *ACS Nano* 9 (2015) 1977–1984.
- [131] X. Long, J. Li, S. Xiao, K. Yan, Z. Wang, H. Chen, S. Yang, *Angew. Chem. Int. Ed.* 53 (2014) 7584–7588.
- [132] J.P. Shi, X.B. Zhou, G.F. Han, M.X. Liu, D.L. Ma, J.Y. Sun, C. Li, Q.Q. Ji, Y. Zhang, X.J. Song, X.Y. Lang, Q. Jiang, Z.F. Liu, Y.F. Zhang, *Adv. Mater. Interfaces* 3 (2016) 1600332.
- [133] X.L. Pan, X.H. Bao, *Chem. Commun.* 47 (2008) 6271–6281.
- [134] Q. Fu, X.H. Bao, *Chem. Soc. Rev.* 46 (2017) 1842–1874.
- [135] X.L. Pan, X.H. Bao, *Acc. Chem. Res.* 44 (2011) 553–562.
- [136] K. Chaitra, P. Sivaraman, R.T. Vinny, U.M. Bhatta, N. Nagaraju, N. Kathyayini, *J. Energy Chem.* 25 (2016) 627–635.
- [137] C.-Y. Su, H. Cheng, W. Li, Z.-Q. Liu, N. Li, Z. Hou, F.-Q. Bai, H.-X. Zhang, T.-Y. Ma, *Adv. Energy Mater.* 7 (2017) 1602420.
- [138] D.H. Deng, L. Yu, X.Q. Chen, G.X. Wang, L. Jin, X.L. Pan, J. Deng, G.Q. Sun, X.H. Bao, *Angew. Chem. Int. Ed.* 52 (2013) 371–375.
- [139] H. Kim, A.W. Robertson, S.O. Kim, J.M. Kim, J.H. Warner, *ACS Nano* 9 (2015) 5947–5957.
- [140] X. Cui, P. Ren, D. Deng, J. Deng, X. Bao, *Energy Environ. Sci.* 9 (2016) 123–129.

- [141] G. Wu, K.L. More, C.M. Johnston, P. Zelenay, *Science* 332 (2011) 443–447.
- [142] H.T. Chung, J.H. Won, P. Zelenay, *Nat. Commun.* 4 (2013) 1922.
- [143] C. Tang, Q. Zhang, *J. Mater. Chem. A* 4 (2016) 4998–5001.
- [144] B.Y. Xia, Y. Yan, N. Li, H.B. Wu, X.W. Lou, X. Wang, *Nat. Energy* 1 (2016) 15006.
- [145] C. Wei, H. Wang, K. Eid, J. Kim, J.H. Kim, Z.A. Alolthman, Y. Yamauchi, L. Wang, *Chem. Eur. J.* 23 (2017) 637–643.
- [146] X. Zhong, Y.Y. Qin, X.L. Chen, W.L. Xu, G.L. Zhuang, X.N. Li, J.G. Wang, *Carbon* 114 (2017) 740–748.
- [147] M. Kuang, Q. Wang, P. Han, G. Zheng, *Adv. Energy Mater.* 7 (2017) 1700193.
- [148] S. Huang, Y. Meng, S. He, A. Goswami, Q. Wu, J. Li, S. Tong, T. Asefa, M. Wu, *Adv. Funct. Mater.* 27 (2017) 1606585.
- [149] K. Qiu, G. Chai, C. Jiang, M. Ling, J. Tang, Z. Guo, *ACS Catal.* 6 (2016) 3558–3568.
- [150] A. Zitolo, V. Goellner, V. Armel, M.T. Sougrati, T. Mineva, L. Stievano, E. Fonda, F. Jaouen, *Nat. Mater.* 14 (2015) 937–942.
- [151] D. Malko, A. Kucernak, T. Lopes, *Nat. Commun.* 7 (2016) 13285.
- [152] J.A. Varnell, E.C.M. Tse, C.E. Schulz, T.T. Fister, R.T. Haasch, J. Timoshenko, A.I. Frenkel, A.A. Gewirth, *Nat. Commun.* 7 (2016) 12582.
- [153] H. Ren, Y. Wang, X. Tang, J. Lu, L. Xiao, L. Zhuang, *J. Energy Chem.* (2017), doi:10.1016/j.jechem.2017.1005.1001.
- [154] F.C. Lei, W. Liu, Y.F. Sun, J.Q. Xu, K.T. Liu, L. Liang, T. Yao, B.C. Pan, S.Q. Wei, Y. Xie, *Nat. Commun.* 7 (2016) 12697.
- [155] T.Y. Ma, S. Dai, S.Z. Qiao, *Mater. Today* 19 (2016) 265–273.
- [156] X.J. Lin, X. Lu, T. Huang, Z.L. Liu, A.S. Yu, *J. Power Sources* 242 (2013) 855–859.
- [157] H.F. Wang, C. Tang, Q. Zhang, *J. Mater. Chem. A* 3 (2015) 16183–16189.
- [158] X.L. Zhu, C. Tang, H.F. Wang, B.Q. Li, Q. Zhang, C.Y. Li, C.H. Yang, F. Wei, *J. Mater. Chem. A* 4 (2016) 7245–7250.
- [159] T.Y. Ma, S. Dai, M. Jaroniec, S.Z. Qiao, *J. Am. Chem. Soc.* 136 (2014) 13925–13931.
- [160] D.U. Lee, J.Y. Choi, K. Feng, H.W. Park, Z.W. Chen, *Adv. Energy Mater.* 4 (2014) 1301389.
- [161] S.C. Du, Z.Y. Ren, J. Wu, W. Xi, H.G. Fu, *Nano Res.* 9 (2016) 2260–2269.
- [162] T.Y. Ma, J.R. Ran, S. Dai, M. Jaroniec, S.Z. Qiao, *Angew. Chem. Int. Ed.* 54 (2015) 4646–4650.
- [163] M.H. Fan, H. Chen, Y.Y. Wu, L.L. Feng, Y.P. Liu, G.D. Li, X.X. Zou, *J. Mater. Chem. A* 3 (2015) 16320–16326.
- [164] B. Li, X.M. Ge, F.W.T. Goh, T.S.A. Hor, D.S. Geng, G.J. Du, Z.L. Liu, J. Zhang, X.G. Liu, Y. Zong, *Nanoscale* 7 (2015) 1830–1838.
- [165] C. Yu, Z.B. Liu, X.T. Han, H.W. Huang, C.T. Zhao, J. Yang, J.S. Qiu, *Carbon* 110 (2016) 1–7.
- [166] Y. Zhang, X. Xia, X. Cao, B. Zhang, N.H. Tiep, H. He, S. Chen, Y. Huang, H.J. Fan, *Adv. Energy Mater.* 7 (2017) 1700220.
- [167] Y. Zhao, C.G. Hu, Y. Hu, H.H. Cheng, G.Q. Shi, L.T. Qu, *Angew. Chem. Int. Ed.* 51 (2012) 11371–11375.
- [168] S. Chen, J.J. Duan, J.R. Ran, M. Jaroniec, S.Z. Qiao, *Energy Environ. Sci.* 6 (2013) 3693–3699.
- [169] Y. Ito, H.J. Qiu, T. Fujita, Y. Tanabe, K. Tanigaki, M.W. Chen, *Adv. Mater.* 26 (2014) 4145–4150.
- [170] Z.P. Chen, W.C. Ren, L.B. Gao, B.L. Liu, S.F. Pei, H.M. Cheng, *Nat. Mater.* 10 (2011) 424–428.
- [171] Y.D. Gao, Y.Y. Zhang, Y. Zhang, L.J. Xie, X.M. Li, F.Y. Su, X.X. Wei, Z.W. Xu, C.M. Chen, R. Cai, *J. Energy Chem.* 25 (2016) 49–54.
- [172] D. Yu, X. He, *J. Appl. Electrochem.* 47 (2017) 13–23.
- [173] X.W. Yu, M. Zhang, W.J. Yuan, G.Q. Shi, *J. Mater. Chem. A* 3 (2015) 6921–6928.
- [174] S. Chen, J.J. Duan, W. Han, S.Z. Qiao, *Chem. Commun.* 50 (2014) 207–209.
- [175] X.W. Yu, M. Zhang, J. Chen, Y.R. Li, G.Q. Shi, *Adv. Energy Mater.* 6 (2016) 1501492.
- [176] X. Xu, Y. Sun, W. Qiao, X. Zhang, X. Chen, X. Song, L. Wu, W. Zhong, Y. Du, *Appl. Surf. Sci.* 396 (2017) 1520–1527.
- [177] L. Zhao, C. Hong, L. Lin, H. Wu, Y. Su, X. Zhang, A. Liu, *Carbon* 116 (2017) 223–231.
- [178] Y.M. Jiang, X. Li, S.J. Yu, L.P. Jia, X.J. Zhao, C.M. Wang, *Adv. Funct. Mater.* 25 (2015) 2693–2700.
- [179] Q. Ding, B. Song, P. Xu, S. Jin, *Chem* 1 (2016) 699–726.
- [180] S.S. Zhou, J.N. Chen, L. Gan, Q. Zhang, Z. Zheng, H.Q. Li, T.Y. Zhai, *Sci. Bull.* 61 (2016) 227–235.
- [181] A.D. Dillon, M.J. Ghidui, A.L. Krick, J. Griggs, S.J. May, Y. Gogotsi, M.W. Barsoum, A.T. Fafarman, *Adv. Funct. Mater.* 26 (2016) 4162–4168.
- [182] J.J. Duan, S. Chen, M. Jaroniec, S.Z. Qiao, *ACS Nano* 9 (2015) 931–940.
- [183] J. Duan, S. Chen, B.A. Chambers, G.G. Andersson, S.Z. Qiao, *Adv. Mater.* 27 (2015) 4234–4241.
- [184] M. Wang, X.D. Wang, M. Chen, Z.Y. Yang, C.Z. Dong, *Chin. J. Catal.* 37 (2016) 1037–1048.
- [185] W. Wang, F. Lv, B. Lei, S. Wan, M.C. Luo, S.J. Guo, *Adv. Mater.* 28 (2016) 10117–10141.
- [186] D.P. He, H.L. Tang, Z.K. Kou, M. Pan, X.L. Sun, J.J. Zhang, S.C. Mu, *Adv. Mater.* 29 (2017) 1601741.
- [187] Z. Yuan, H.-J. Peng, T.-Z. Hou, J.-Q. Huang, C.-M. Chen, D.-W. Wang, X.-B. Cheng, F. Wei, Q. Zhang, *Nano Lett.* 16 (2016) 519–527.
- [188] W. Chen, Y.F. Gong, J.H. Liu, *Chin. Chem. Lett.* 28 (2017) 709–718.
- [189] J.Q. Huang, Q. Zhang, F. Wei, *Energy Storage Mater.* 1 (2015) 127–145.
- [190] K.P. Gong, F. Du, Z.H. Xia, M. Durstock, L.M. Dai, *Science* 323 (2009) 760–764.
- [191] Y. Zhao, R. Nakamura, K. Kamiya, S. Nakanishi, K. Hashimoto, *Nat. Commun.* 4 (2013) 2390.
- [192] Y. Jiao, Y. Zheng, K. Davey, S.Z. Qiao, *Nat. Energy* 1 (2016) 16130.
- [193] J. Zhang, Z. Zhao, Z. Xia, L. Dai, *Nat. Nanotechnol.* 10 (2015) 444–452.
- [194] J. Zhang, L. Qu, G. Shi, J. Liu, J. Chen, L. Dai, *Angew. Chem. Int. Ed.* 55 (2016) 2230–2234.
- [195] Y. Zheng, Y. Jiao, Y.H. Zhu, L.H. Li, Y. Han, Y. Chen, A.J. Du, M. Jaroniec, S.Z. Qiao, *Nat. Commun.* 5 (2014) 3783.
- [196] D. Yan, Y. Li, J. Huo, R. Chen, L. Dai, S. Wang, *Adv. Mater.* 27 (2017) 1606459.
- [197] J.J. Wu, M.T.F. Rodrigues, R. Vajtai, P.M. Ajayan, *Adv. Mater.* 28 (2016) 6239–6246.
- [198] M.Q. Guo, J.Q. Huang, X.Y. Kong, H.J. Peng, H. Shut, F.Y. Qian, L. Zhu, W.C. Zhu, Q. Zhang, *New Carbon Mater.* 31 (2016) 352–362.
- [199] L.M. Dai, Y.H. Xue, L.T. Qu, H.J. Choi, J.B. Baek, *Chem. Rev.* 115 (2015) 4823–4892.
- [200] F. Hasche, M. Oezaslan, P. Strasser, T.P. Fellinger, *J. Energy Chem.* 25 (2016) 251–257.
- [201] L.P. Zhang, W.S. Jia, X.F. Liu, J.Z. Li, M.M. Titirici, *J. Energy Chem.* 25 (2016) 566–570.
- [202] T.T. Zhang, C.S. He, L.B. Li, Y.Q. Lin, *Chin. J. Catal.* 37 (2016) 1275–1282.
- [203] Y.Y. Li, L. Wang, X.M. He, B. Tang, Y.X. Jin, J.L. Wang, *J. Energy Chem.* 25 (2016) 131–135.
- [204] S.H. Li, L. Ding, L.Z. Fan, *Sci. China Chem.* 58 (2015) 417–424.
- [205] W.J. Lee, J. Lim, S.O. Kim, *Small Methods* 1 (2017) 1600014.
- [206] J.L. Shi, H.F. Wang, X.L. Zhu, C.M. Chen, X. Huang, X.D. Zhang, B.Q. Li, C. Tang, Q. Zhang, *Carbon* 103 (2016) 36–44.
- [207] D.S. Yu, Q. Zhang, L.M. Dai, *J. Am. Chem. Soc.* 132 (2010) 15127–15129.
- [208] C.-Y. Chen, C. Tang, H.-F. Wang, C.-M. Chen, X. Zhang, X. Huang, Q. Zhang, *ChemSusChem* 9 (2016) 1194–1199.
- [209] M. Li, Z. Liu, F. Wang, J. Xuan, *J. Energy Chem.* 26 (2017) 422–427.
- [210] M.T. Li, L.P. Zhang, Q. Xu, J.B. Niu, Z.H. Xia, *J. Catal.* 314 (2014) 66–72.
- [211] J. Wang, Z.X. Wu, L.L. Han, Y.Y. Liu, J.P. Guo, H.L.L. Xin, D.L. Wang, *Chin. Chem. Lett.* 27 (2016) 597–601.
- [212] K.H. Wu, D.W. Wang, X. Zong, B.S. Zhang, Y.F. Liu, I.R. Gentle, D.S. Su, *J. Mater. Chem. A* 5 (2017) 3239–3248.
- [213] G.P. Hao, N.R. Sahaie, Q. Zhang, S. Krause, M. Oschatz, A. Bachmatiuk, P. Strasser, S. Kaskel, *Chem. Commun.* 51 (2015) 17285–17288.
- [214] M. Qiao, C. Tang, L.C. Tanase, C.M. Teodorescu, C. Chen, Q. Zhang, M.-M. Titirici, *Mater. Horizons* (2017), doi:10.1039/C7MH00298J.
- [215] Y.Z. Liu, Y.F. Li, F.Y. Su, L.J. Xie, Q.Q. Kong, X.M. Li, J.G. Gao, C.M. Chen, *Energy Storage Mater.* 2 (2016) 69–75.
- [216] Y.K. Zhou, X. Xu, B. Shan, Y.W. Wen, T.T. Jiang, J.M. Lu, S.W. Zhang, D.P. Wilkinson, J.J. Zhang, Y.H. Huang, *Energy Storage Mater.* 1 (2015) 103–111.
- [217] L. Wei, H.E. Karahan, S.L. Zhai, Y. Yuan, Q.H. Qian, K.L. Goh, A.K. Ng, Y. Chen, *J. Energy Chem.* 25 (2016) 191–198.
- [218] L. Zhang, J. Niu, M. Li, Z. Xia, *J. Phys. Chem. C* 118 (2014) 3545–3553.
- [219] J. Liang, Y. Jiao, M. Jaroniec, S.Z. Qiao, *Angew. Chem. Int. Ed.* 51 (2012) 11496–11500.
- [220] Y. Zheng, Y. Jiao, L. Ge, M. Jaroniec, S.Z. Qiao, *Angew. Chem. Int. Ed.* 52 (2013) 3110–3116.
- [221] S. Chen, J.J. Duan, M. Jaroniec, S.Z. Qiao, *Adv. Mater.* 26 (2014) 2925–2930.
- [222] S. Chen, J. Duan, Y. Zheng, X. Chen, X.W. Du, M. Jaroniec, S.-Z. Qiao, *Energy Storage Mater.* 1 (2015) 17–24.
- [223] Y.P. Zhu, Y. Jing, A. Vasileff, T. Heine, S.Z. Qiao, *Adv. Energy Mater.* 7 (2017) 1602928.
- [224] T. Sun, Q. Wu, Y. Jiang, Z. Zhang, L. Du, L. Yang, X. Wang, Z. Hu, *Chem. Eur. J.* 22 (2016) 10326–10329.
- [225] J.T. Zhang, L.M. Dai, *Angew. Chem. Int. Ed.* 55 (2016) 13296–13300.
- [226] C. Hu, L. Dai, *Adv. Mater.* 29 (2017) 1604942.
- [227] Y. Zheng, Y. Jiao, L.H. Li, T. Xing, Y. Chen, M. Jaroniec, S.Z. Qiao, *ACS Nano* 8 (2014) 5290–5296.
- [228] S. Buller, J. Strunk, *J. Energy Chem.* 25 (2016) 171–190.
- [229] M. Qiao, C. Tang, G. He, K. Qiu, R. Binions, I.P. Parkin, Q. Zhang, Z. Guo, M.M. Titirici, *J. Mater. Chem. A* 4 (2016) 12658–12666.
- [230] G.L. Tian, Q. Zhang, B.S. Zhang, Y.G. Jin, J.Q. Huang, D.S. Su, F. Wei, *Adv. Funct. Mater.* 24 (2014) 5956–5961.
- [231] G.L. Tian, M.Q. Zhao, D.S. Yu, X.Y. Kong, J.Q. Huang, Q. Zhang, F. Wei, *Small* 10 (2014) 2251–2259.
- [232] J.-L. Shi, G.-L. Tian, Q. Zhang, M.-Q. Zhao, F. Wei, *Carbon* 93 (2015) 702–712.
- [233] X.-B. Cheng, Q. Zhang, H.-F. Wang, G.-L. Tian, J.-Q. Huang, H.-J. Peng, M.-Q. Zhao, F. Wei, *Catal. Today* 249 (2015) 244–251.
- [234] K. Preuss, V.K. Kannuchamy, A. Marinovic, M. Isaacs, K. Wilson, I. Abrahams, M.M. Titirici, *J. Energy Chem.* 25 (2016) 228–235.
- [235] M. Sereydych, K. Laszlo, E. Rodriguez-Castellon, T.J. Bandoz, *J. Energy Chem.* 25 (2016) 236–245.
- [236] B. Huang, L. Peng, F. Yang, Y. Liu, Z. Xie, *J. Energy Chem.* 26 (2017), doi:10.1016/j.jechem.2017.1003.1016.
- [237] W. Ding, Z.D. Wei, S.G. Chen, X.Q. Qi, T. Yang, J.S. Hu, D. Wang, L.J. Wan, S.F. Alvi, L. Li, *Angew. Chem. Int. Ed.* 52 (2013) 11755–11759.
- [238] H.W. Liang, X.D. Zhuang, S. Bruller, X.L. Feng, K. Mullen, *Nat. Commun.* 5 (2014) 4973.
- [239] W. Ding, L. Li, K. Xiong, Y. Wang, W. Li, Y. Nie, S.G. Chen, X.Q. Qi, Z.D. Wei, *J. Am. Chem. Soc.* 137 (2015) 5414–5420.
- [240] S. Li, C. Cheng, H.-W. Liang, X. Feng, A. Thomas, *Adv. Mater.* 29 (2017) 1700707.
- [241] F. Banhart, J. Kotakoski, A.V. Krasheinnikov, *ACS Nano* 5 (2011) 26–41.
- [242] L. Vicarelli, S.J. Heerema, C. Dekker, H.W. Zandbergen, *ACS Nano* 9 (2015) 3428–3435.
- [243] Y. Jiang, L. Yang, T. Sun, J. Zhao, Z. Lyu, O. Zhuo, X. Wang, Q. Wu, J. Ma, Z. Hu, *ACS Catal.* 5 (2015) 6707–6712.

- [244] Y. Ito, Y.H. Shen, D. Hojo, Y. Itagaki, T. Fujita, L.H. Chen, T. Aida, Z. Tang, T. Adschiri, M.W. Chen, *Adv. Mater.* 28 (2016) 10644–10651.
- [245] Y. Jia, L.Z. Zhang, A.J. Du, G.P. Gao, J. Chen, X.C. Yan, C.L. Brown, X.D. Yao, *Adv. Mater.* 28 (2016) 9532–9538.
- [246] L. Tao, Q. Wang, S. Dou, Z. Ma, J. Huo, S. Wang, L. Dai, *Chem. Commun.* 52 (2016) 2764–2767.
- [247] Z. Liu, Z. Zhao, Y. Wang, S. Dou, D. Yan, D. Liu, Z. Xia, S. Wang, *Adv. Mater.* 29 (2017) 1606207.
- [248] H.-F. Wang, C. Tang, Q. Zhang, *Catal. Today* (2017), doi:10.1016/j.cattod.2017.1002.1012.
- [249] Y.Y. Wang, Y.Q. Zhang, Z.J. Liu, C. Xie, S. Feng, D.D. Liu, M.F. Shao, S.Y. Wang, *Angew. Chem. Int. Ed.* 56 (2017) 5867–5871.
- [250] D.L. Carroll, P. Redlich, P.M. Ajayan, J.C. Charlier, X. Blase, A. DeVita, R. Car, *Phys. Rev. Lett.* 78 (1997) 2811–2814.
- [251] P.J. Britto, K.S.V. Santhanam, A. Rubio, J.A. Alonso, P.M. Ajayan, *Adv. Mater.* 11 (1999) 154–157.
- [252] P. Zhang, X.L. Hou, J.L. Mi, Y.Q. He, L. Lin, Q. Jiang, M.D. Dong, *Phys. Chem. Chem. Phys.* 16 (2014) 17479–17486.
- [253] G.-L. Chai, Z. Hou, D.-J. Shu, T. Ikeda, K. Terakura, *J. Am. Chem. Soc.* 136 (2014) 13629–13640.
- [254] L. Zhang, Q. Xu, J. Niu, Z. Xia, *Phys. Chem. Chem. Phys.* 17 (2015) 16733–16743.
- [255] X. Wang, X. Li, C. Ouyang, Z. Li, S. Dou, Z. Ma, L. Tao, J. Huo, S. Wang, *J. Mater. Chem. A* 4 (2016) 9370–9374.
- [256] S. Kattel, G. Wang, *J. Mater. Chem. A* 1 (2013) 10790–10797.